Fizika Nizkikh Temperatur, 2006, v. 32, No. 11, p. 1382–1401

Fourier transform infrared studies of the N_2–O_2 binary system

M. Minenko and H.-J. Jodl

TU Kaiserslautern, Department of Physics, Erwin Schrödinger Str., Kaiserslautern 67663, Germany
E-mail: jodl@physik.uni-kl.de

Received May 26, 2006

Solid solutions $(N_2)_x(O_2)_{1-x}$ have been investigated by infrared absorption measurements mainly in the O_2 and N_2 stretching regions, between 60–10 K, completing former similar studies by Raman scattering. We produced thermodynamically stable samples by a careful thermal treatment, followed by cooling/heating cycles over weeks, during which we took spectra. From fingerprints in infrared spectra we deduce phase transition lines, solubility lines and suggest a refined, improved T–x% phase diagram with respect to inconsistencies between those in literature. Spectra of N_2–O_2 mixtures are pretty complex but referring to known spectra of pure systems N_2 or O_2 we were able to assign and interpret broad ($\sim$100 cm^{-1}) phonon side bands to fundamentals and electronic transition (O_2) depending on actual temperature and concentration. Narrow features in spectra (<10 cm^{-1}) were attributed to the vibron DOS of N_2 or O_2, whose bandwidth, band shape and intensity are different and characteristic for each phase. Differences between pure and mixed systems were pointed out. Matrix isolation technique (2 ppm of CO) was used to probe our mixture.

PACS: **81.30.–t**, 64.70.Kb, **64.75.+g**, **78.30.–j**, 63.20.Ls

Keywords: infrared absorbtion, Fourier-transform infrared technique, vibrational and exitonic region.

1. Introduction

Molecular crystals (rare gases, H_2, N_2, O_2, CO, CO_2 ...) have been studied extensively since 1950 by all kinds of technique like spectroscopy, structural studies, thermodynamic investigations, molecular dynamics simulation. At least two directions of research can be identified: molecular solids as matrix material or as simple model systems for solid state aspects. Mixtures of these components were much less studied on the contrary, because of several reasons: due to the complexity in results after pure systems, due to missing theoretical modeling, due to problems in producing samples with sufficiently good crystal quality. In a recent paper [1] we could prove that discrepancies in published phase diagrams T–x% of N_2–O_2 [2,3] are most likely due to thermodynamic instable samples. The general aim of this paper [1] was to deduce from fingerprints in vibron and phonon spectra lines of phase transitions, to prove reproducibility and reliability of our statements by cooling/heating cycles, to determine quantitatively from relative Raman vibron band intensities the solubility of N_2 in O_2 or vice versa. In paper [1] we reported only about results from Raman spectra.

With respect to Raman and infrared (IR) activity of elementary excitations it is more than obvious to study N_2–O_2 mixture spectroscopically by Raman scattering. However, due to the admixing of elements in the phases based on the other element some elementary excitations gain IR activity; in addition one may expect IR active combinations of excitations. Of course, this induced IR absorption is weak, but modern Fourier-transform infrared (FTIR) technique is pretty sensitive. Therefore in comparison to Raman scattering FTIR spectra contain much more information.

The only spectroscopic paper — besides those on excitonic transitions in O_2 molecules [4] — is a far-IR absorption analysis in solid N_2–O_2 solutions [5]. But the observed transition in phonon spectra from the N_2 translations ($T_u^- \sim 52$ cm^{-1}, $T_u^+ \sim 73$ cm^{-1}), which are IR active, to O_2 phonons (~ 55 cm^{-1}, ~ 80 cm^{-1}), which are only Raman but not IR active, by increasing the oxygen concentration must be considered with many doubts. We could not find any IR active transla-

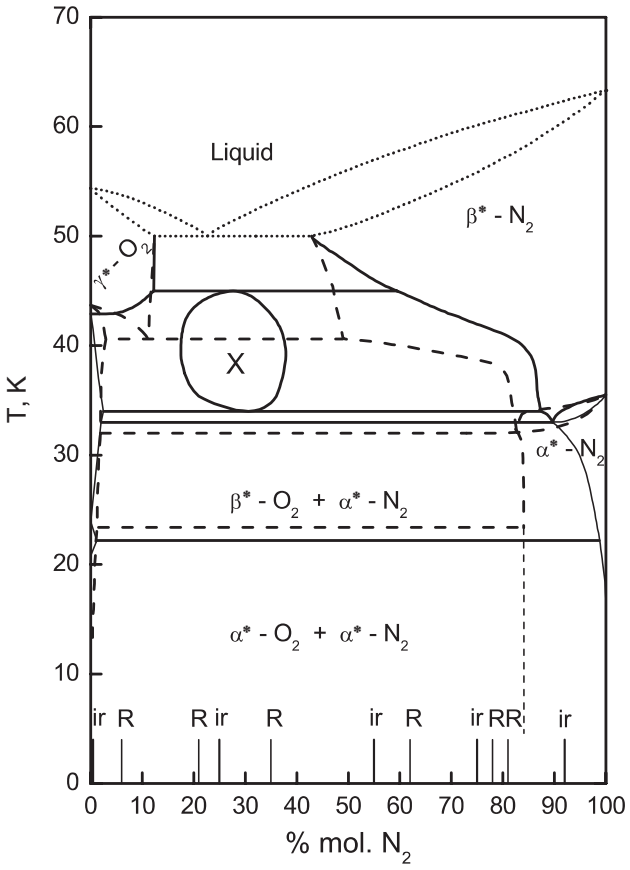

Fig. 1. T–concentration (*x*%) phase diagram for N_2–O_2 from structural analysis reported by two different groups (solid lines by [3], broken lines by [2]; liquid region – dots – is taken from [2], the authors: M. Ruheman, H. Lichter, and P. Komarov, *Phys. Z. Sovjetunion* **8**, 326 (1935)). We studied several concentrations by Raman scattering (R [1]) and by FTIR absorption (ir).

tions in far-IR spectra of thick solid samples of α-O_2, as it is expected from group theory. Also the second statement in [5] about the tuning of the magnon intensity in α-O_2 by doping with N_2 impurities (10% to 50%) is also more than questionable; because it is agreed now [1–3] that only less or about 1% of N_2 can be solved in α^*-O_2. Therefore only the magnon absorption of pure O_2 and the one with $\leq$ 1% N_2 should be compared.

In our analysis of spectra of N_2–O_2 mixtures we will base on comparison with spectra of pure O_2 and pure N_2 [6–8] that were studied quite good up to now.

Publications on the binary system $(N_2)_x(O_2)_{1-x}$ with aim to determine the *T*-*x*% phase diagram are based on structural analysis. Figure 1 shows versions of Barrett, Meyer [3] and of Baryl'nik, Prokhvatilov [2], which are obviously different with respect to the existence of the *X*-phase, temperatures of phase transitions and solubility of oxygen in nitrogen phases. By our indirect method via optical spectroscopy we want to clarify these differences or open questions.

What are the aims of this paper? First of all we have to produce thermodynamically equilibrated samples checking their quality by means of optical spectroscopy. That means to find proper cooling and warming rates and to check hysteresis effects and reproducibility of spectra. Second, we plan to deduce from FTIR spectra in the vibrational and excitonic region indirectly the *T*–*x*% diagram. In pure systems clear changes in spectra are seen on the way through phase transitions and we do believe to recognize the same in mixtures. As the third aim we consider the determination of solubility of O_2 in α^*-N_2 phase being one of the most obvious discrepancies between the two existing variants of the *T*–*x*% diagram. And finally, we want to detect all changes in spectra of mixtures in comparison with spectra of pure systems.

2. Experimental

Nitrogen (99.999%) and oxygen (99.998%) were premixed in a relatively large vessel in the desired composition (via partial pressures) at room temperature. The mixture remained there for 2–3 days for homogenous mixing before loading the optical cell. This cell with sample chamber (∅ 10 mm, thickness 1.2 mm), equipped with sapphire windows, was mounted on a cold finger of a closed-cycle He cryostat. To avoid partial demixing in the gas-liquid region (see Fig. 2 [1]) and via contact between vapors over the sample and the gas mixing system we followed here another strategy. The cell temperature was set at T = 11 K, and the cell was filled with the immediately freezing gaseous mixture (couple of seconds), so that there was no chance for a concentration change. Then the cell was disconnected from the gas mixing system. Samples were warmed up to the liquid phase and were annealed for a couple of hours. Then we cooled the samples through the liquid-solid phase transition simultaneously measuring spectra. About 1 K below the transition temperature samples were annealed again for few hours. During the very slow cooling (0.5–0.1 K/h) of samples, we controlled their optical quality by measuring their total light transmission. We achieved to cool down the samples to 11 K with good optical quality.

Temperature was determined by a calibrated Si-diode attached directly to the optical cell with an absolute accuracy of the sample temperature determination of about 0.1 K in the whole temperature range studied here (11–60 K).

Spectra in the vicinity of the O_2 fundamental ($\sim$ 1600 cm^{-1}), N_2 fundamental ($\sim$ 2300 cm^{-1}), their combination and the electronic transition in oxygen ($\Sigma \rightarrow \Delta$ at 8000 cm^{-1}) were recorded by a Fourier spectrometer (Bruker IFS 120 HR). The following light

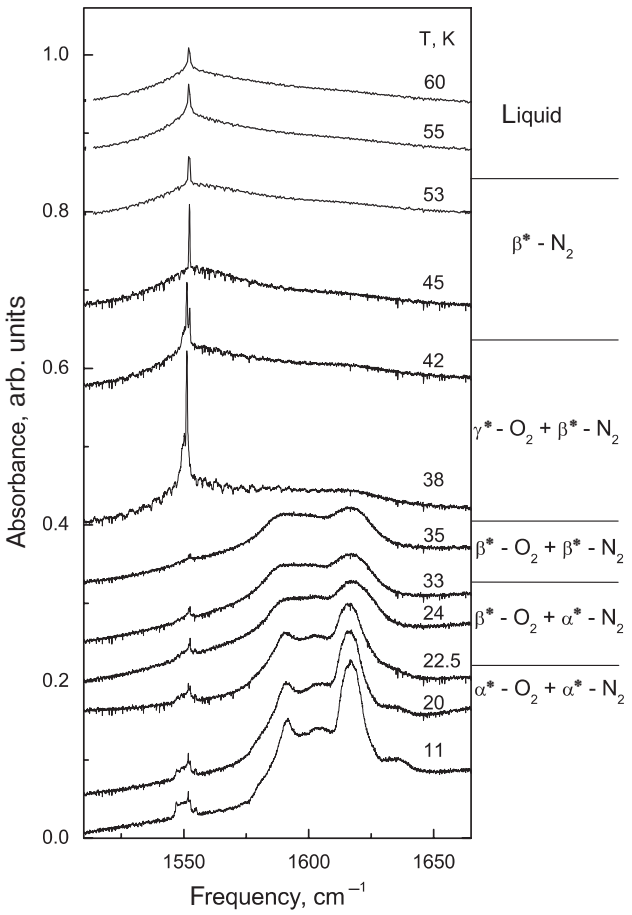

Fig. 2. Absorption spectra in the region of oxygen fundamental (~ 1550 cm^{-1}) as a function of temperature, collected during the warming cycle of $(N_2)_{0.55}(O_2)_{0.45}$ mixture. Different phases are indicated on the right side. (Details of this overview are presented in the following Figs. 3–5).

sources and beam splitters were used: a glowbar source and a KBr beam splitter (spectral range 800–5000 cm^{-1}) as well as a tungsten lamp and a CaF_2 beam splitter (spectral range 1900–11000 cm^{-1}). Liquid-N_2-cooled InSb and MCT detectors were used. Frequency resolution was varied from 0.015 cm^{-1} to 1 cm^{-1} depending on the band width of investigated spectral lines; frequency accuracy was 0.01 cm^{-1} due to used interference pattern of the He gas laser. The empty optical cell delivered the reference spectrum.

The actual concentration $(N_2)_x(O_2)_{1-x}$ was controlled after measurements by evaporating the sample into a test volume. This sample gas was then analyzed by means of chromatography and mass-spectrometry. This actual concentration and the concentration of the initial mixture, determined by partial pressures, almost coincided and the error in concentration is ≤ 1 mol %.

In Fig. 1, showing the existing variants of the phase diagram T–x% we marked the 5 different mixtures studied by means of FTIR spectroscopy as well as 6 mixtures studied by means of Raman spectroscopy [1]. Our variant of the phase diagram is based therefore on data from all 11 measured mixtures.

3. Results and spectra

In the following we will present IR spectra of excitations in our samples from lower to higher frequencies. Although these spectra at first glance look pretty complex and manifold they can be unambiguously assigned primarily by comparing them with similar spectra of the pure systems (O_2 and N_2). The evolution of spectra with temperature during warming cycles will be described in detail and changes in spectra document phase transitions. Topics of more common interest like solubility, metastability/hysteresis or vibron density of states will be discussed later.

3.1. Oxygen fundamental region (~ 1550 cm^{-1})

Figure 2 shows for one selected concentration $(N_2)_{0.55}(O_2)_{0.45}$ the changes in spectra in the region of the O_2 stretching band and its phonon combination band (side band, SB) during warming. Lines on the right hand side of this figure separate phase regions. Since the overview of spectra is pretty overcharged, we use in the next figures enlargements to show details along with the text.

Liquid phase and β^*-N_2*

The only spectral features, which can be identified between 60 and 43 K, are a relatively narrow band (band width 1–2 cm^{-1}) at 1552 cm^{-1} on top of a broad band, which is very similar to the SB in liquid or γ-O_2 (see Fig. 3). We assign these features to the IR absorption of the O_2 fundamental (stretching band or vibration) in liquid mixture and in β^*-N_2 plus side band to it. The symmetric stretching of O_2 molecules (the narrow band) becomes IR active due to a symmetry breaking in the molecule's environment in mixture. The difference between spectra in liquid and in the β^*-N_2 phase can be seen in Fig. 3. The broad wings on both sides of the fundamental are typical for liquids [9] and are generally assigned to the rotational diffusion excited via vibration/rotation coupling. In β^*-N_2 the narrow band seems to be not connected with the

* A star is commonly used to characterize the phase in mixture; without it one deals with a pure system.

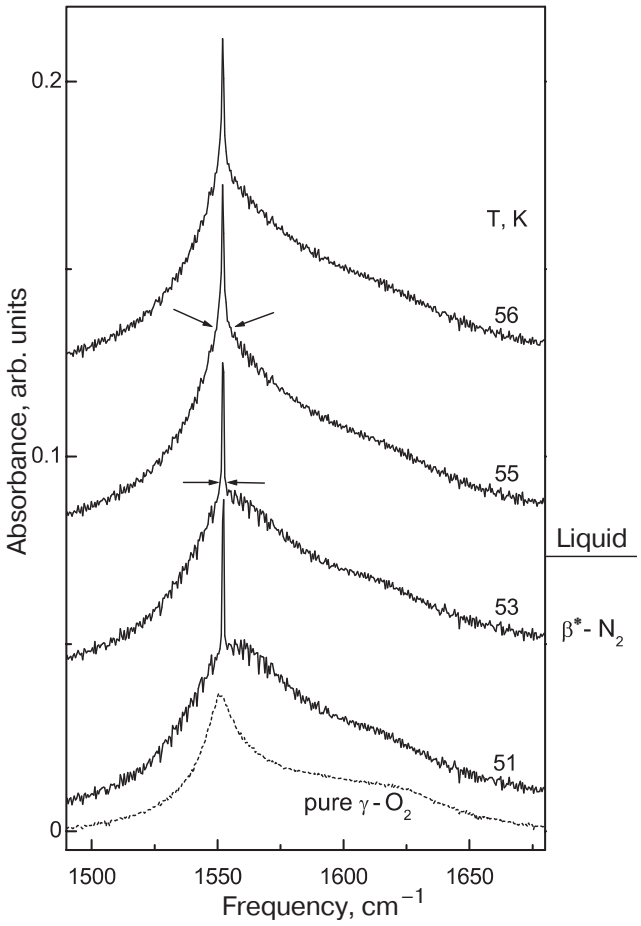

Fig. 3. Absorption spectra in the region of oxygen vibration of the liquid mixture and of β^*-N_2. Subtle changes of the fundamental mode (bandwidth, band shape) are stressed by arrows. Spectrum from pure γ-O_2 (T = 44 K) is added for comparison.

broad band (SB). An unambiguous deconvolution of SB in plastic phases is hindered by a variety of different types of motion, each possessing a broad band of energies, and their specific interactions. In both oxygen and nitrogen the biggest role are playing rotational (±30 cm^{-1} around the fundamental) and translational (centered at +65 cm^{-1}) motions. From the similarity with the SB in γ-O_2 we can deduce that O_2 molecules imbedded in γ^*-O_2 or in β^*-N_2 structure participate in similar types of motion.

Due to our measurements at different concentrations (liquid + β-N_2) two-phase region is a bit more narrow (in temperatures) than in the phase diagram by Barrett–Meyer. We confirm that the maximal solubility of O_2 in β^*-N_2 is around 55% (see Fig. 1).

γ^*-O_2

Starting from T = 42 K the narrow band (< 1 cm^{-1}) at 1552 cm^{-1} (band *1* in Fig. 4) is getting weaker and on the low-frequency side appears a broader band (~ 3–4 cm^{-1}) which includes a narrow (< 1 cm^{-1}) feature at 1551 cm^{-1} (band *2* in Fig. 4). The broad feature (SB) gains some intensity at about 60–70 cm^{-1} on the Stokes side of the zero-phonon band increasing the similarity of this band with the side band in pure γ-O_2. We assign band *2* to the defect-induced IR absorption of the O_2 vibration or, in other words, to a smeared out vibron DOS in γ^*-O_2 (see section 4.2). The intensity of that band is quite substantial due to the relatively high solubility (~ 10%) of nitrogen in γ^*-O_2 that means that practically each O_2 molecule has at least one N_2 molecule as a neighbor. At lower temperatures band *2* is more pronounced, whereas the band at 1552 cm^{-1} (band *1*) almost vanishes (assigned to the vibration of O_2 molecules in β^*-N_2).

So from Fig. 4 one can derive that at the concentration $(N_2)_{0.55}$ $(O_2)_{0.45}$ γ^*-O_2 phase surely exists in the temperature interval (38–42 K). From the decrease of the band *1* intensity we conclude that solubility of O_2 in β^*-N_2 strongly depends on temperature; namely, it is decreasing lowering temperature. The exact range of the β^*-N_2 phase existence should be cleared out with

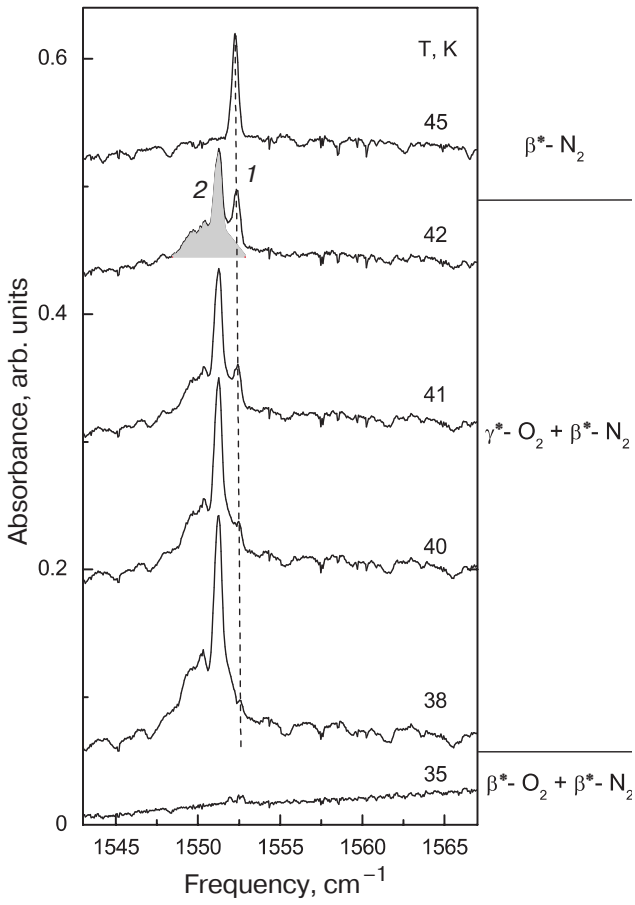

Fig. 4. The same spectra, as in Fig. 2, but in a more narrow frequency range, demonstrate changes of the fundamental only: band *1* is the IR absorption of O_2 solved in β^*-N_2, band *2* (shaded area) represents the vibron DOS of γ^*-O_2.

the help of the analysis of spectra in the N_2 stretching band vicinity (see later).

In this range our variant of the phase diagram (Fig. 21) differs strongly from both previous (Fig. 1). Neither in infrared, nor in Raman studies we found any evidence for the *X*-phase. γ^*-O_2 phase was found at temperatures as low as 37.5 K (warming cycle value).

β^*-O_2

At T = 35 K both narrow band(s) in the vicinity of the O_2 stretching band (Fig. 4) and broad phonon band on its Stokes side (Fig. 2) differ substantially from all the spectra at higher temperatures. The phonon side band is now very similar to the one in β-O_2 [6,7]. The band at the O_2 vibration is much less intensive and consists actually out of three features (this could be seen better in Fig. 5 at lower temperatures): a plateau (1547–1553 cm^{-1}) with maximum at about 1552 cm^{-1} and a very narrow peak (< 0.2 cm^{-1}) at 1552.5 cm^{-1} (both are tentatively assigned to the impurity-induced vibron DOS of β^*-O_2); at 1552.7 cm^{-1} (T = 35 K) the already known band *1* (vibration of O_2 molecules in β^*-N_2 , band width < 1 cm^{-1}). The evolution of the band *1* with temperature is better seen in a more N_2-rich sample $(N_2)_{0.92}(O_2)_{0.08}$ (Fig. 6). The (α^*– β^*)-N_2 phase transition at $T \sim 34$ K can be identified due to a jump in the band frequency, band width and changes in band shape. One can recognize only a very weak response from the β^*-O_2 phase since the O_2 concentration is low and the amount of the O_2 phase is even smaller. Between 34.6 and 36 K β^*-O_2 phase disappears and only β^*-N_2 remains.

The jump in frequency ($\Delta\omega_{tr}$) of the O_2 stretching band in nitrogen at the (α^*–β^*)-N_2 phase transition phase can be estimated comparing the values of the environmental shifts in nitrogen phases (at the transition temperature) from [7]:

$$\Delta\omega_{tr} \sim \Delta\omega_{env}(\alpha^*\text{-}N_2) - \Delta\omega_{env}(\beta^*\text{-}N_2) =$$

$$= -1.8 - (-2.4) = 0.6 \text{ cm}^{-1},$$

$$\Delta\omega_{tr}\,(\text{exp}) = 1.2 \text{ cm}^{-1}.$$

It should be noticed that the used values for the environmental shifts correspond to undistorted structures. The larger experimental jump value can be ex-

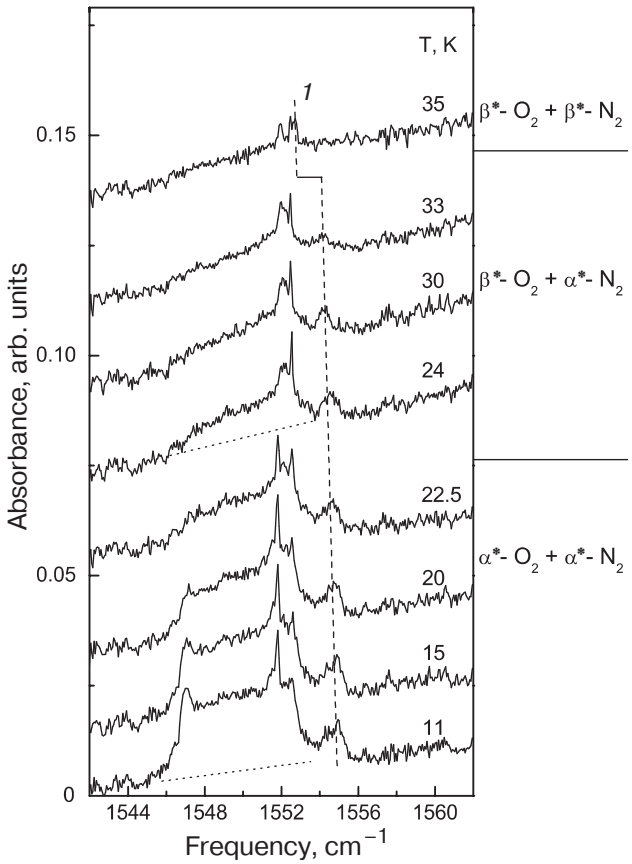

Fig. 5. The same part of spectra like in Fig. 4 at lower temperatures. Dotted lines are baselines for vibron DOS in β^*-O_2 and α^*-O_2. Broken line follows the evolution of the band *1* (O_2 in β^*- and α^*-N_2).

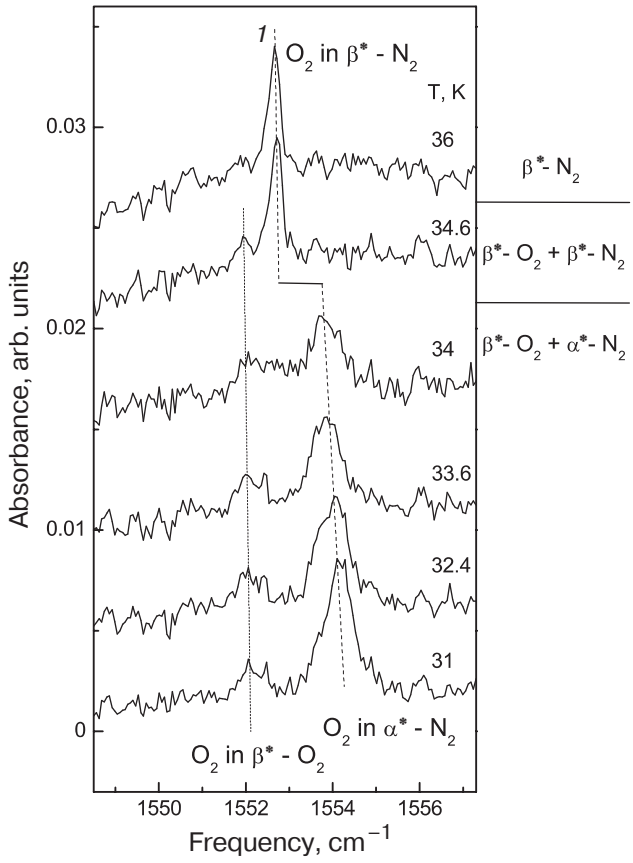

Fig. 6. Spectra of $(N_2)_{0.92}(O_2)_{0.08}$ in a narrow frequency range around O_2 fundamental. Broken line as in Fig. 5 follows band *1*. Dotted line follows a weak absorption of O_2 in β^*-O_2.

plained by an influence of dissolved molecules (e.g., by a variation in their amount), and would hint on a jump in solubility of oxygen during the (α^*–β^*)-N_2 phase transition.

From spectra of O_2 vibration and its phonon side band we were able to detect not only (γ^*–β^*)-O_2 phase transition but also (α^*–β^*)-N_2. Spectral fingerprints confirm the phase mixture of β^*-O_2 and β^*-N_2 in the temperature range 34–36.5 K that is closer to the variant of Barrett—Meyer but is not as narrow as theirs (Figs. 1, 21).

α^*-O_2

At T = 22.5 K the phonon SB starts getting more pronounced and maxima, known from the SB of pure α-O_2 [6,7], can be recognized, although these features are impurity-broadened (Fig. 2). The band at the fundamental contains additional features in comparison to spectra of β^*-O_2. The broad band between 1546 and 1553 cm^{-1} is gaining intensity and becomes plateau-like at 11 K (Fig. 5); intensity of the narrow feature at 1552.5 cm^{-1} is decreasing lowering temperature, whereas a new narrow (< 0.2 cm^{-1}) feature at 1552 cm^{-1} is showing up in α^*-O_2 . It looks as if both decrease/increase evolutions in intensities of these bands are linked together. We assign ~ 7 cm^{-1} broad band together with these narrow features to the vibron DOS of α^*-O_2 ; for discussion see later. Band *1* at 1554.7 cm^{-1} (T = 11 K) is still present (assigned to O_2 molecules in α^*-N_2).

Temperature of the (β^*–α^*)-O_2 phase transition (T ~ 23 K) according to us is lying somewhere between the values from two previous phase diagram variants (Fig. 1).

3.2. Nitrogen fundamental region (~ 2330 cm^{-1})

An overview of spectra in the region of the N_2 stretching band as a function of temperature (52–12 K) during cooling for one concentration $(N_2)_{0.92}(O_2)_{0.08}$ is shown in Fig. 7. Since the phonon side band of N_2 is much less intensive than the one of O_2 we are forced to choose a nitrogen-rich mixture in order to demonstrate changes in this side band.

Changes in the closest vicinity of the N_2 stretching band with temperature are demonstrated by spectra of the $(N_2)_{0.55}(O_2)_{0.45}$ mixture (Fig. 8), which undergoes more phase transitions than the N_2-rich sample does.

β^*-N_2

Spectra of the side band in β^*-N_2 phase (Fig. 7) can be deconvoluted in a narrow (< 1 cm^{-1}) peak-like band at ~ 2327 cm^{-1}, broad (~ 30–40 cm^{-1}) bands centered at about 2345 cm^{-1}, 2390 cm^{-1} and in low-temperature β^*-N_2 another one around the stretching band frequency 2327 cm^{-1}. We assign the narrow spectral component to the impurity-induced vibron density of states in β^*-N_2 (for details see Sec. 4.2). A smeared out peak of matrix-isolated CO_2 at ~ 2347 cm^{-1} (ν_3 mode) is also present in our spectra (a star in Fig. 7) together with its very weak side band. These 3 broad bands in this mixture are similar to excitations in pure β-N_2 [7] and in N_2–Ar [10]. Therefore we were able to achieve a consistent deconvolution of spectra into the induced fundamental and the phonon side bands. The band at ~ 60 cm^{-1} with respect to the zero-phonon line (ZPL; ν_0 ~ 2327 cm^{-1}) is due to translational contributions to the phonon sideband. The band at ~ 15–20 cm^{-1} we associate, due to literature, with the nutational motion of molecules

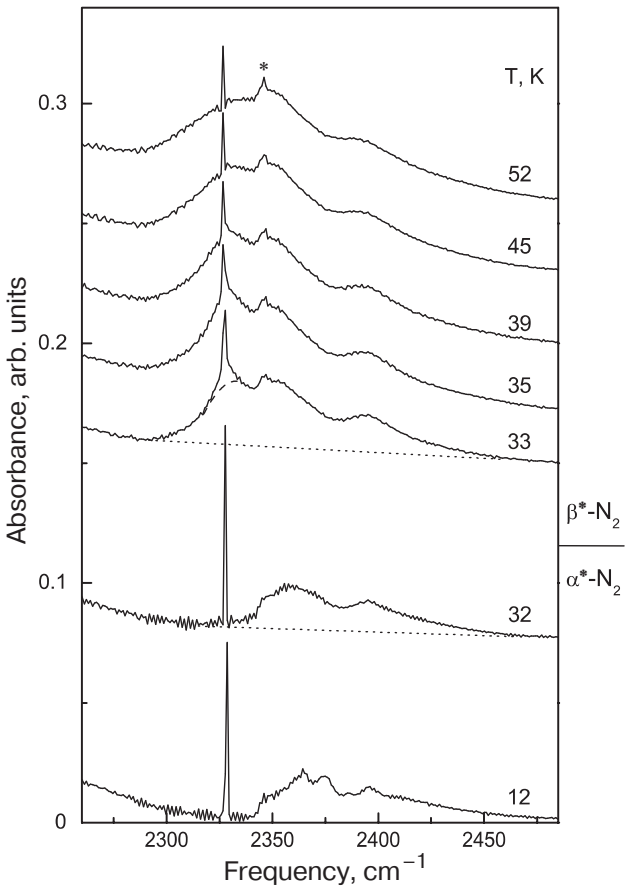

Fig. 7. Absorption spectra in the region of nitrogen fundamental (~ 2330 cm^{-1}) as a function of temperature collected during the cooling cycle of $(N_2)_{0.92}(O_2)_{0.08}$ mixture. Different phases are indicated on the right side. The broad bands (phonon side band) are distinctly changing lowering temperature. Dotted lines serves as baseline of side bands. Changes of the band shape near the N_2 fundamental inside of β*-N_2 are stressed by a broken line (spectrum at 33 K), which repeats the shape in high-temperature β*-N_2. Peak assigned by a star (*) is due to absorption of CO_2 (~ ppm; ν_3 mode).

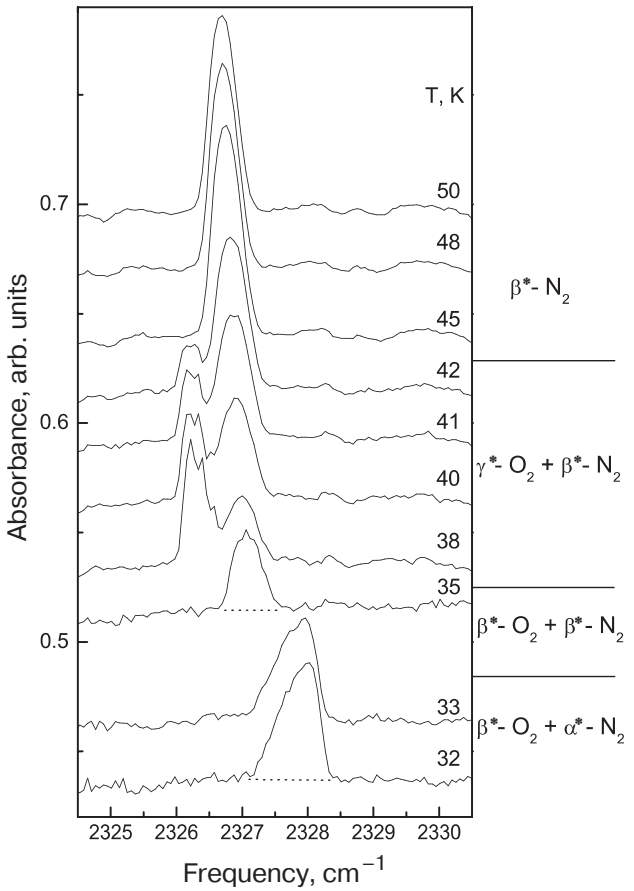

Fig. 8. Spectra of $(N_2)_{0.55}(O_2)_{0.45}$ mixture in a narrow frequency range. Dotted lines are baselines for vibron DOS in β^*- and α^*-N_2. A band with 3 peaks at lower frequencies is the IR absorption of N_2 solved in γ^*-O_2.

(correlated orientational oscillation of molecular axes relative to the *c* axes of hcp structure [11]) or to librational jumps [12]. The remaining broad band, centered at ZPL, present only in low-temperature β-N_2, arises probably due to a partial freezing of the nutational motion (glassy β-N_2).

β^*-N_2 is the only phase between 53 and 43 K in $(N_2)_{0.55}(O_2)_{0.45}$ mixture and between 60 and ~ 35 K in $(N_2)_{0.92}(O_2)_{0.08}$ mixture.

γ^*-O_2 *and* β^*-N_2

An additional structured band at 2326–2327 cm^{-1} with 3 maxima separated by less than 0.2 cm^{-1} is present between 42 and 38 K in spectra of $(N_2)_{0.55}(O_2)_{0.45}$ mixture (Fig. 8). They exist at cooling and at warming in the temperature interval of phase coexistence of γ^*-O_2 and β^*-N_2. The signal/noise ratio unambiguously emphasizes the existence of several peaks. The fact that frequencies of these peaks are slightly changing with temperature also confirms the physical origin of these peaks.

One expects in this temperature interval in O_2-rich mixtures either γ^*-O_2 or an *X*-phase in coexistence with β^*-N_2 (Fig. 1). But we did not find any spectral evidence for the *X*-phase. Since this structured band represents vibrations of nitrogen molecules and since the solubility of N_2 in γ^*-O_2 is expected to be quite high (10–12% [2,3]), we assign the new band to vibrations of N_2 molecules in γ^*-O_2. The nature of the infrared activity is usual for mixtures; it is a broken symmetry of the molecules' environment in the host crystal. But what is the origin of 3 peaks?

The γ-O_2 is a phase with 8 molecules per cell: two molecules on site **a** (sphere-like) and 6 molecules on site **c** (disk-like) [13]. The splitting of the Raman-active O_2 vibron is about 1.2 cm^{-1} [14]. One may imagine that N_2 molecules may occupy these two different sites. But an energy splitting due to sites is too large in comparison to separation of 3 maxima (~ 0.2 cm^{-1}). On the other hand it is known from experiments on N_2–Ar, that the monomer/dimer splitting is about 0.15 cm^{-1} [15]. Since the solubility of N_2 in γ^*-O_2 is 10–12% (Fig. 1), the probability to find a dimer or a trimer of N_2 molecules in γ^*-O_2 ($Pm3n$) is substantial (30%). Then a possible explanation of the triplet would be the different number of nitrogen molecules among nearest neighbors of the oscillating N_2 molecule: none, one or two. But we should also take in account that due to the existence of different sites there is a number of combinations for the pair of N_2 molecules: sphere—sphere, sphere—disk or disk—disk.

At T = 35 K we observe only one narrow (0.5 cm^{-1}) band at 2327 cm^{-1}, which we assign to the induced vibron DOS of β^*-N_2 (Fig. 8).

As a consequence of these spectral findings we can specify in the T–x% diagram the area of phase coexistence of γ^*-O_2 and β^*-N_2 (see Fig. 21). Since we did not find any spectroscopic response from N_2 in β^*-O_2 we confirm a weak (~ 1%) solubility of N_2 in β^*-O_2.

α^*-N_2

Below 34.5 K in α^*-N_2 the spectral features are getting more pronounced. The induced stretching band, which is symmetric in the β^*-phase and centered at 2327 cm^{-1} (T > 33.5 K), is now asymmetric in the α^*-phase with a maximum at about 2328 cm^{-1} (T < 33.5 K) (Fig. 8) (details on vibron DOS in Sec. 4.2). To higher frequencies with respect to the fundamental mode (or ZPL) we register a broad band with two maxima (+ 30 and + 65 cm^{-1}), which we assign to be the smeared out phonon side band known from pure α-N_2 [16,17]. Theoretically determined DOS of lattice modes of α-N_2 [17] associate the first maximum at 30–35 cm^{-1} to lattice modes with the librational character, the second maximum at

+ 60 cm^{-1} to lattice modes with the translational character.

Bands centered near the fundamental and at about + 20 cm^{-1} (T = 35 K) disappear at the (β^*–α^*)-N_2 phase transition completely (Fig. 7). In orientationally ordered α^*-N_2 the nutations are frozen out. The orientational motion is represented by librations.

There is no indication of the (β^*–α^*)-O_2 phase transition in spectra of the N_2 fundamental region at ~ 2320 cm^{-1} (estimated value: $\omega_{gas} - \Delta\omega_{env}$). With our very sensitive FTIR technique we do not observe any fingerprints of N_2 solved in α^*- and β^*-O_2 in spectra. Taking in account our signal/noise ratio we agree with previous investigators that the solubility of N_2 in α^*- and β^*-O_2 is about or less than 1% (see Fig. 1).

3.3. Overtone region (3000–5000 cm^{-1})

In pure systems phonon side bands to the overtones (ZPL (0-2) + SB) are 100 times less intense than side bands to the fundamental. We do not observe these structures here because our samples were relatively thin (~ 1 mm). But at low temperatures we observe two relatively narrow bands in that overtone region.

At 4656–4657 cm^{-1} we detect a band (width ~ 1 cm^{-1}), which vanishes at the (α^*–β^*)-N_2 phase transition. The overview spectra as a function of temperature during warming for the concentration $(N_2)_{0.92}(O_2)_{0.08}$ is shown in Fig. 9,*a*. The assignment is obvious comparing this spectrum with the one in pure α-N_2 (Fig. 9,*b*). Legay [18] modeled this band in pure N_2 as follows: in α-N_2 with 4 molecules per unit cell two neighboring molecules can perform a simultaneous out of phase vibration ((0–1)A_g symmetry and (0–1)T_g symmetry); this combined excitation — called two-vibron — is IR active; whereas in β-N_2 such excitation is not expected because there exists only one stretching mode (Fig. 9,*a*). The case in mixture is similar in principle, but the spectrum is slightly broader and more smeared out (Fig. 9,*b*) due to impurities (O_2 in α^*-N_2). Legay [18] gave a full description of the IR absorption: band position, band shape, integrated intensity and assignment with respect to Raman active modes (A_g, T_g). The position of this two-vibron excitation in pure α-N_2 (T = 11 K) can be estimated qualitatively as follows:

$$\omega_{min} = \omega_{Raman}(A_g) + \omega_{Raman}(T_g) =$$
$$= 2327.6 + 2328.6 = 4656.2 \text{ cm}^{-1},$$

$$\omega_{max} = 4657.4 \text{ cm}^{-1}.$$

In our case ω_{min} (exp) ~ 4656.5 cm^{-1} and ω_{max} (exp) = = 4657.5 cm^{-1}.

Therefore we confirm the model of Legay, which can be extended to mixtures considering that a part

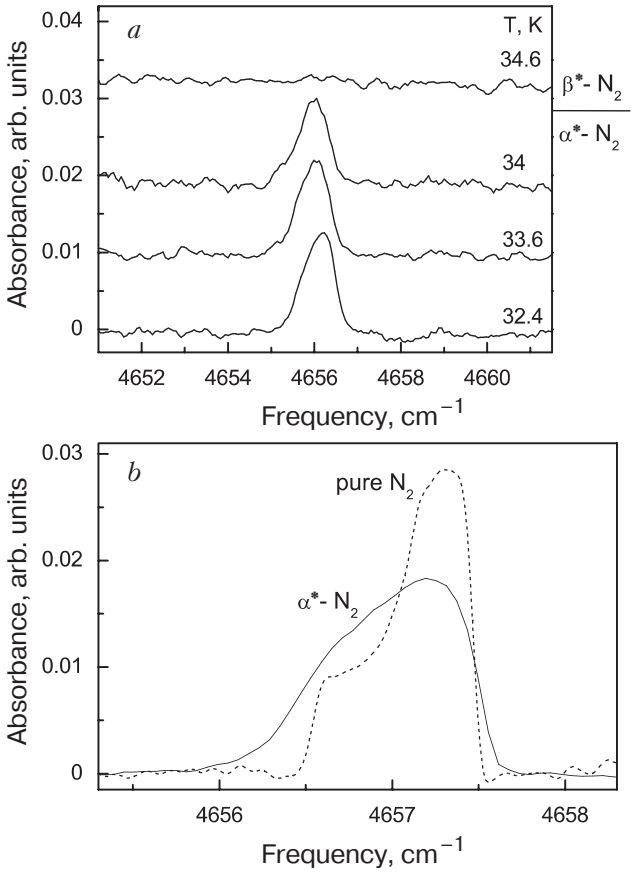

Fig. 9. Overview of absorption spectra in the region of the two-vibron ((0–1) N_2 + (0–1) N_2) ~ 4600 cm^{-1} around (α^*–β^*)-N_2 transition temperature, collected during the warming cycle of $(N_2)_{0.92}(O_2)_{0.08}$ mixture (*a*); comparison of two-vibron in pure N_2 (broken line) and in α^*-N_2 (T = = 11 K) (*b*).

of the band's integrated intensity is defect-induced. This spectral fingerprint is a good indicator of the (α^*–β^*)-N_2 phase transition: from Fig. 9,*a* follows that it occurs between 34 and 34.6 K at this concentration.

At 3883–3884 cm^{-1} we detect another band (Fig. 10), which we assign to a simultaneous combined («mixed») excitation of the N_2 (0–1) and O_2 (0–1) vibrations in α^*-N_2. Since the solubility of O_2 in α^*-N_2 was approximated by 5–8% [1] and less than 1% of N_2 is soluble in β^*- and α^*-O_2 we believe that this «mixed» excitation is taking place in α^*-N_2 only. This conclusion is supported by the increase of the band intensity with an increase of the N_2 concentration and thus of the α^*-N_2 amount. In order to estimate the approximate frequency of such band we just add frequencies of corresponding vibrations:

$$\omega_{N2+O2} = \omega_R (A_g \text{ or } T_g\ N_2) + \omega\ (O_2 \text{ in } \alpha^*\text{-}N_2) =$$
$$= 2327.6 \text{ or } 2328.6 + 1554.7 = 3882.3\text{–}3883.3 \text{ cm}^{-1},$$

in comparison to ω (exp) = 3882.5–3884.2 cm^{-1}.

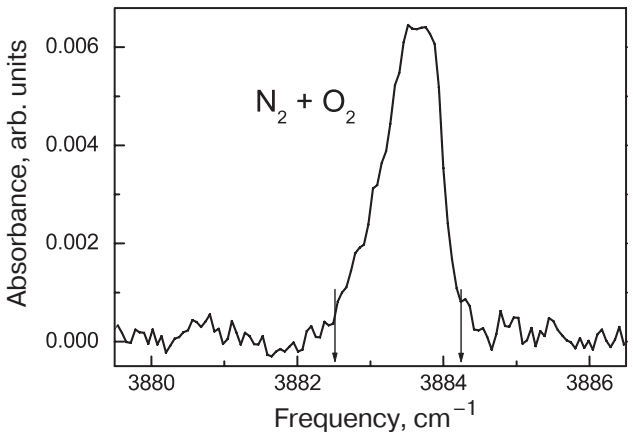

Fig. 10. Spectrum of a «mixed» two-vibron ((0–1) N_2 + + (0–1) O_2) in $(N_2)_{0.92}(O_2)_{0.08}$ mixture at T = 11 K. Arrows indicate ω_{min} and ω_{max}.

The intensity ratio of this N_2+O_2 band and the N_2–N_2 two-vibron band is 1:3, whereas one would expect a much weaker intensity of the «mixed» band due to a low amount of oxygen in α^*-N_2 . Obviously it is compensated by the induced dipole moment due to a large distortion of the symmetry of the O_2 molecules' environment caused by a presence of other O_2 molecules among the host (N_2) ones.

The integrated intensity of two-vibron bands ($I \sim \eta^2$, η is an orientational order parameter) allows us to discuss the orientational ordering between neighboring molecules [19]. In Fig. 11 we plotted temperature dependences of the reduced orientational order parameter of oxygen (△) and nitrogen (○) in α^*-N_2 and of nitrogen in pure N_2 (solid line). While N_2 molecules are almost as oriented as in the pure system till relatively high temperatures, O_2 molecules, possessing a much smaller electric quadrupole moment, are considerably less oriented in α^*-N_2. It is well known that orientational order in α-N_2 is predominantly caused by the electric quadrupole–quadrupole interaction between nitrogen molecules.

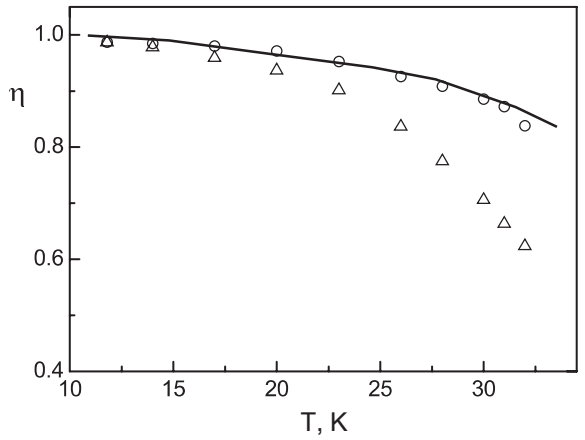

Fig. 11. Reduced orientational order parameter ($\eta(T)/\eta$ (11 K)) as a function of temperature: triangles — O_2 molecules and circles — N_2 molecules in the mixture $(N_2)_{0.92}(O_2)_{0.08}$, solid line — pure N_2 [19].

3.4. Exciton region of oxygen (~ 8000 cm^{-1})

The absorption bands of the pure electronic and electonic-vibronic transitions (phonon side bands to them) in solid oxygen are already well studied [4], also as a function of temperature [8] and pressure [20]. We concentrate here on the lowest energy transition ${}^3\Sigma_g^-(v=0) \rightarrow {}^1\Delta_g(v=0)$. In α-O_2 this band has a fine structure: the strongest peculiarities are assigned to the exciton–magnon bound state [4]. The zero phonon line (ZPL) of this band was determined recently [8]. This made possible an assignment of other peculiarities. The spectrum of $(N_2)_{0.92}(O_2)_{0.08}$ mixture at T = 11 K in comparison with the one of pure oxygen (with reduced intensity) is shown in Fig. 12. The band in mixture is clearly smeared out so that some features of the above mentioned fine structure are not resolved. In general, the band shape is comparable with spectra of pure O_2 at T = 20–22 K. There are two additional weak bands on the anti-Stokes side that are making the difference (arrows in Fig. 12, see also Fig. 14). Electronic absorption bands are characteristic for a phase and thus could serve as a good indicator of phase transitions. The existence in a mixture of a band, which is similar to the one in α-O_2 , gives us a right to claim the existence of the α^*-O_2 in this mixture at a given temperature (11 K). This observation means that the solubility of O_2 in α^*-N_2 is less than O_2 concentration (8%) in this mixture. Spectra in earlier works [4] should be reinterpreted with the knowledge of the new solubility value at low temperatures (see Sec. 4.1).

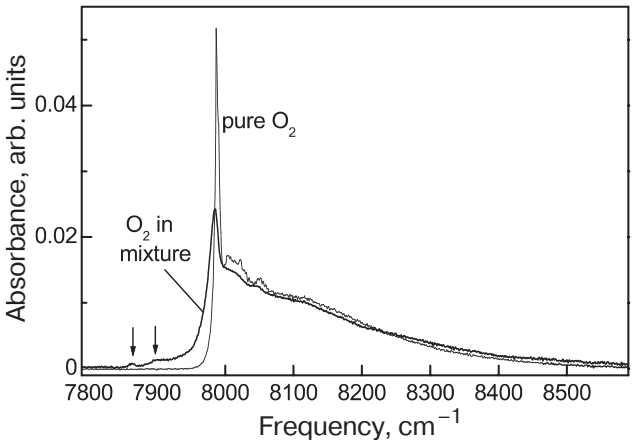

Fig. 12. Comparison of electronic absorption of O_2 molecules ($\Sigma \rightarrow \Delta$) in pure α-O_2 (thin line) with reduced intensity and in mixture at T = 11 K. Arrows point on the contribution from O_2 in α^*-N_2 on the anti-Stokes side of the spectrum in mixture.

An overview of spectra at different temperatures (11–50 K) during warming of the $(N_2)_{0.92}(O_2)_{0.08}$ mixture is shown in Fig. 13. We have discussed already the spectrum in α^*-O_2. At the $(\alpha^*$–$\beta^*)$-O_2 phase transition this band transforms in a broad featureless asymmetric band, typical for β-O_2; its maximum jumps for about 80 cm^{-1} to lower frequencies. These changes are explained by the loss of the long-range magnetic order [8]. The spectrum at T = 23 K mirrors the superposition of two phases, confirming the $(\alpha^*$–$\beta^*)$-O_2 phase transition at $T \le 23$ K. But the spectrum at T = 41 K differs from all others substantially: its intensity is in the order of magnitude smaller than those of bands in β^*-O_2. Whereas intensity of electronic bands in pure γ-O_2 is only three times smaller than in β-O_2 [8]. In addition the band maximum of spectrum at 41 K in mixture is moved for about 50 cm^{-1} to lower frequencies from the value in γ-O_2. So if this band cannot be linked to the γ^*-O_2 phase it must be formed by oxygen molecules embedded in β^*-N_2 phase. Therefore we are able to claim that there is no oxygen-based phase in $(N_2)_{0.92}(O_2)_{0.08}$ mixture at T = 41 K; that is in agreement with the phase diagrams in Fig. 1 and is confirmed by our spectra in the fundamental region.

Now, after identifying a spectrum of the electronic excitation of oxygen molecules imbedded in the nitrogen phase, we can return to the discussion of the anti-Stokes wing of the spectrum at T = 11 K (Fig. 14). The spectrum of pure O_2 at T = 22 K serves as a measure of broadening of the main band from O_2 in α^*-O_2 and can be taken as a tentative baseline for IR absorption in this frequency range. Spectrum at T = 41 K (assigned to absorption of O_2 in β^*-N_2) is shown for comparison: intensity of the whole band is comparable with intensity of the anti-Stokes side of the spectrum at 11 K and frequency of the band's maximum lies between those two features of the low-temperature spectrum. Thus we assign the big part of intensity on the anti-Stokes wing of the spectrum at 11 K to the electronic excitation of O_2 molecules dissolved in α^*-N_2 (7864 cm^{-1} – first feature) and its combination with phonons of this phase (phonon side band), the most prominent of which (at +32 and

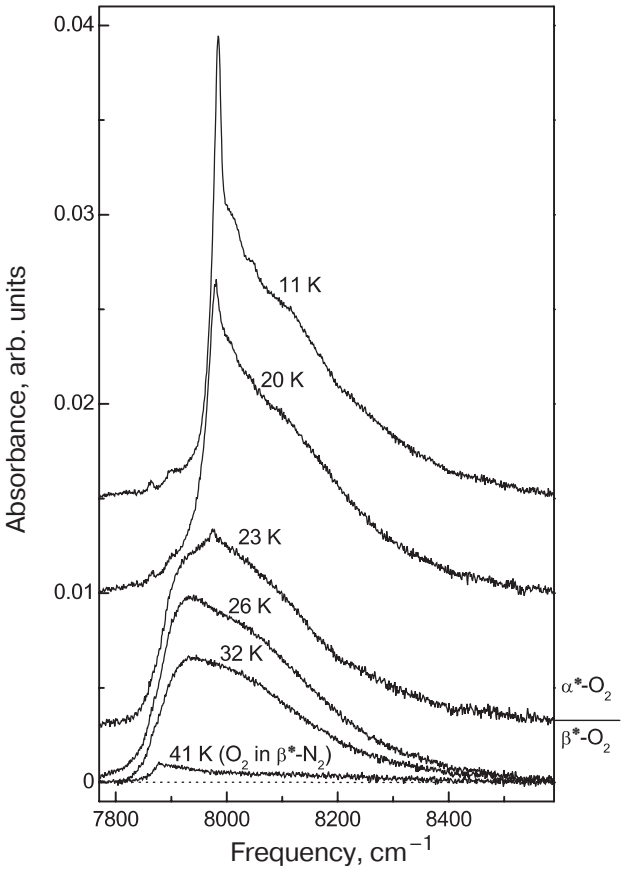

Fig. 13. Evolution of electronic spectra with temperature of $(N_2)_{0.92}(O_2)_{0.08}$ mixture. Please note the distinct change in absorbance for O_2 solved in β^*-N_2 (T = 41 K).

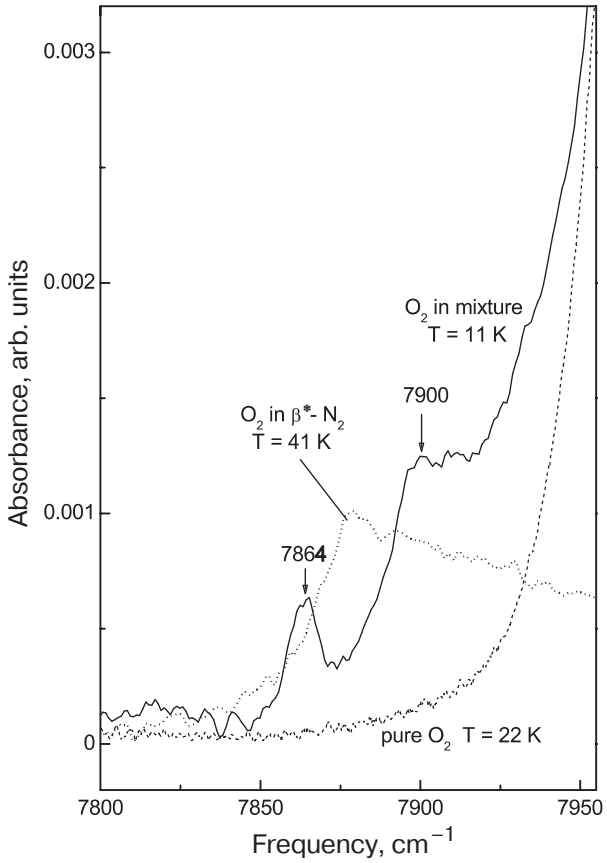

Fig. 14. Details of spectra on the anti-Stokes side of ZPL: solid line — mixture at T = 11 K (see Fig. 12), broken line — pure O_2 at T = 22 K, dotted line — O_2 solved in β^*-N_2 at 41 K (see Fig. 13). Arrows indicate band maxima (see text).

+38 cm^{-1}; librons [21]) are seen as the second feature at 7900 cm^{-1}. Therefore the whole band at T = 11 K represents a superposition of the absorption of O_2 molecules in α^*-N_2 and in α^*-O_2.

Electronic transition bands of O_2 appeared to be very useful spectral fingerprints in studies of the N_2–O_2 phase diagram. The shape of the band and its intensity tell us whether oxygen molecules form their own (O_2-rich) phase or they are dissolved in the N_2-rich phase. And as in the pure O_2 we can trace phase transitions from changes in spectroscopic characteristics of the electronic bands. Moreover, one can obtain valuable information about the solubility of O_2 in N_2 at a given temperature (details in 4.1).

4. Discussion

4.1. Phase diagram T–x%

Phase transitions lines. In Sec. 3 we already described how one can deduce from changes in spectra of different modes the phase transitions in N_2–O_2 mixtures. Here we would like to summarize the results outlining the most suitable excitations for demonstration of the main transitions: $\alpha \rightarrow \beta \rightarrow \gamma$ in O_2 and $\alpha \rightarrow \beta$ in N_2. We put the stress on differences with previous phase diagrams (Fig. 1), preparation and thermal treatment of samples and we discuss solubility of oxygen in nitrogen-rich phases that is one of the most prominent deviations between two previous variants of the diagram.

The (α^*–β^*)-O_2 transition ($T \sim 23$ K) in N_2–O_2 is seen the best from changes in spectra of electronic transition ($\Sigma \rightarrow \Delta$, ~ 8000 cm^{-1}). The frequency jump of the band origin ($\Delta \sim 90$ cm^{-1}) and drastic changes in band shape can be explained by magnetism of α-O_2 [8]. The phase transition temperature differs just marginally (< 1 K) from literature values [2,3].

The (β^*–γ^*)-O_2 transition ($T \sim 37$ K) in our mixture is well documented by changes in spectra of the O_2 fundamental and its phonon side band ($\nu_0 \sim 1550$ cm^{-1}): like in the pure case, changes in the SB shape are accompanied by a frequency shift of the band maximum. In addition in γ^*-O_2 we can see a very intensive induced vibron band. The phase transition temperature differs substantially (4–8 K) both from literature data and from the one in pure O_2 ($T \sim 43.8$ K). Due to difficulties to obtain thermodynamically stable samples at cooling we took into consideration only the transition temperature recorded at warming.

The (α^*–β^*)-N_2 transition ($T \sim 34$ K) can be followed in several ways: changes in spectra of the side band to the N_2 fundamental, of the two-vibron band and of the induced vibron band (~ 2328 cm^{-1}). As an example, the phase coexistence of α^*- and β^*-N_2 is demonstrated in Fig. 15 between 34 and 34.6 K in a N_2-rich mixture during warming.

We claim $T \approx 34$ K to be the (α^*–β^*)-N_2 phase transition temperature for a wide range of concentrations, i.e., the horizontal line in the T–x% diagram, separating the two-phase regions. That is 1–2 K higher than in previous diagrams (Figs. 1, 21).

Phase transitions lines, found by two groups on the basis of structural studies [2,3], are shown in Fig. 1. In these publications neither the history of samples, nor the path in the T–x% diagram, nor the time of temperature changes are mentioned. Our studies revealed that the temperature of a phase transition depends sensitively on the fact, whether this transition was monitored during cooling or warming cycle, on the rate of temperature changes and on the annealing time.

Differences in spectra during cooling and warming cycles are well documented in Figs. 16, 17; considering as example the most problematic phase transitions (β^*–γ^*)-O_2 and (α^*–β^*)-N_2. The induced O_2 vibron band (around 1550 cm^{-1}) and its phonon side band are

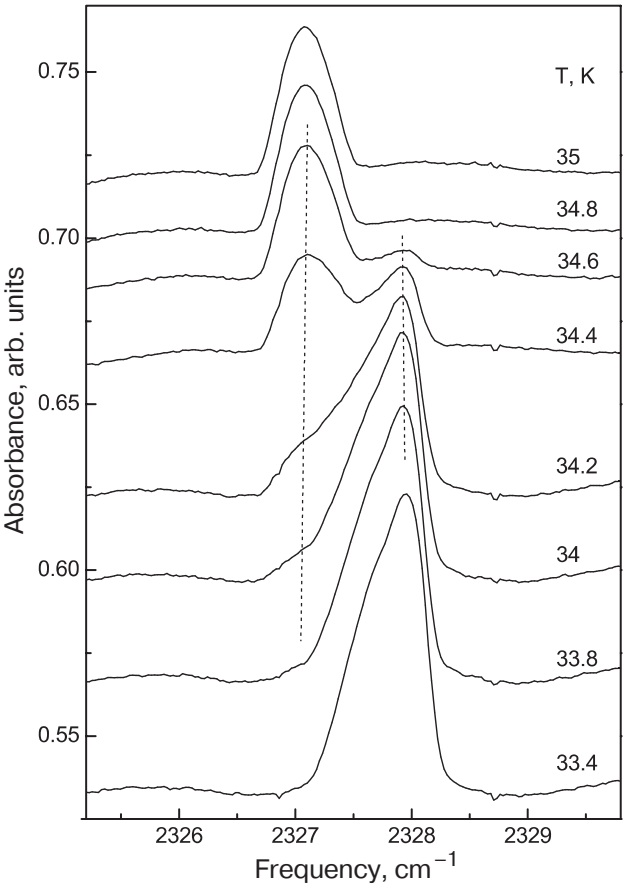

Fig. 15. Absorption spectra in the region of nitrogen fundamental (~ 2328 cm^{-1}) as a function of temperature, collected during the warming cycle of $(N_2)_{0.92}(O_2)_{0.08}$ mixture. In this narrow temperature interval the coexistence of phases (α^*+ β^*)-N_2 is demonstrated.

shown in Fig. 16. Changes in shape and intensity of the side band during cooling between T = 32 and 31 K and during warming between T = 35 and 38 K indicate the (β^*–γ^*)-O_2 phase transition. We were not able to reduce this difference in transition temperature (~ 5 K) although we changed temperature quite slowly (hours/K) and we annealed the sample for several hours before each measurement. This phenomenon could be explained as follows. Solubility of N_2 in γ^*-O_2 (~ 10%) differs substantially from the one in β^*-O_2 (~ 1%). Therefore during the (γ^*–β^*)-O_2 phase transition a massive demixing of nitrogen from the oxygen phase should take place, but it is hindered by a low rate of diffusion at these relatively low temperatures. The system becomes undercooled; there is not enough energy for the phase transition.

Spectra in Fig. 17, that were taken simultaneously with those in Fig. 16, document similar discrepancies for warming/cooling cycles in the vicinity of the impurity-induced N_2 vibron band. During cooling the (β^*–α^*)-N_2 phase transition occurs simultaneously with the (γ^*–β^*)-O_2 transition between 32 and 31 K. Whereas during warming they are clearly separated: we register the (α^*–β^*)-N_2 transition between 33 and 35 K and the (β^*–γ^*)-O_2 transition happens between 35 and 38 K.

So the message is: the difference between transition temperatures in our studies and the ones in literature could be due to the difficulty to achieve thermodynamically stable samples that was, most likely, not realized in earlier investigations.

X-phase and solubility. There are two further open questions in the published T–x% diagrams [2,3]: an X-phase [3] and solubility of oxygen in N_2-rich phases.

We have studied 5 concentrations $(N_2)_x(O_2)_{1-x}$ by means of infrared absorption and we have not detected any sign in spectra which might be brought in relation with an X-phase. All the spectra in these mixtures can be traced back to phases of pure systems. Therefore we claim that the T–x% diagram at ambient pressure consists only of known phases of the pure systems.

There is a big discrepancy in literature in solubility of oxygen in α^*-N_2 determined by structural studies: one group [3] predicted a strong decrease in solubility from ~ 10% at the (α^*–β^*)-N_2 phase transition (~ 34 K) to less than 1% at about 20 K, another group [2] claimed it to be as large as 18% and independent on temperature.

There are two ways to study solubility by means of spectroscopy. The obvious one is to prepare samples with different concentrations and to search for a concentration, at which a certain phase (documented by

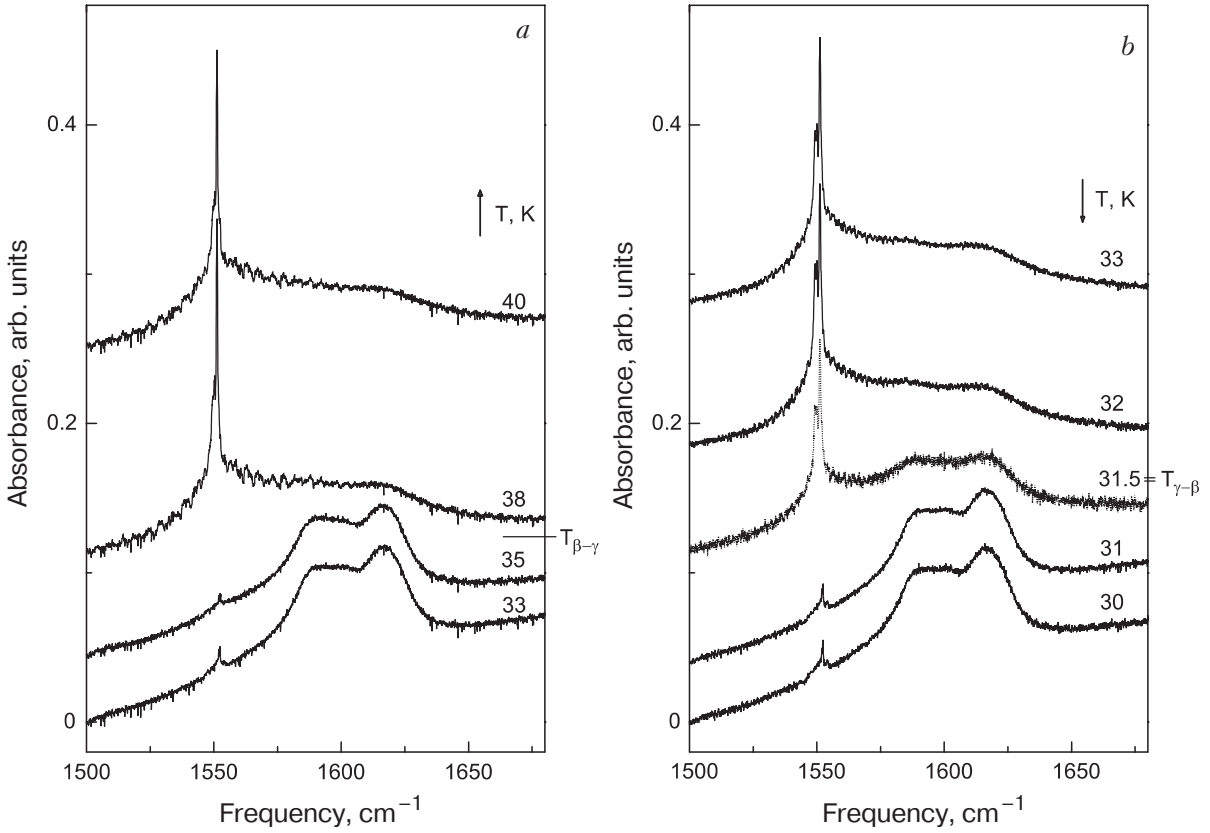

Fig. 16. Spectra of $(N_2)_{0.55}(O_2)_{0.45}$ mixture in the region of oxygen fundamental recorded during warming (*a*) and cooling cycles (*b*).

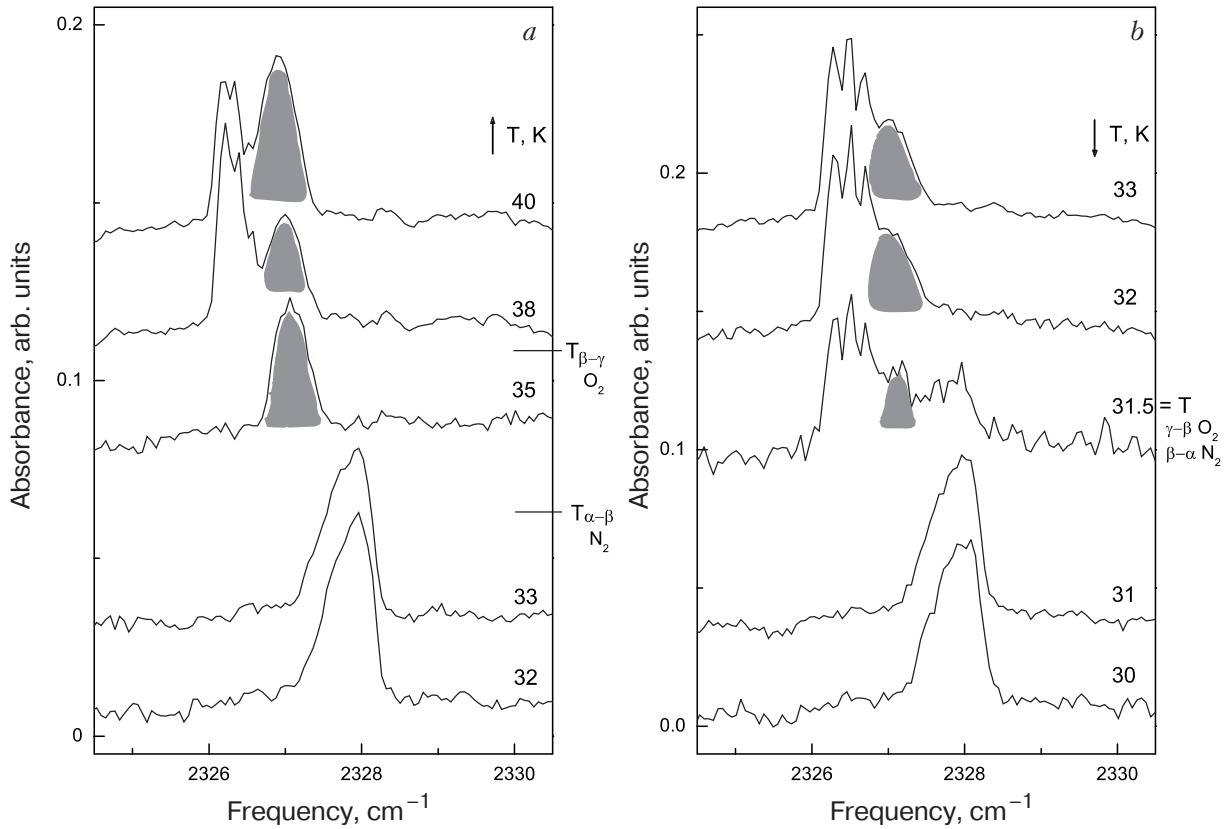

Fig. 17. Spectra of $(N_2)_{0.55}(O_2)_{0.45}$ mixture in the region of nitrogen fundamental recorded during warming (*a*) and cooling (*b*) cycles confirm Fig. 16 and demonstrate that (β^*–α^*)-N_2 transition at cooling occurs simultaneously with (γ^*–β^*)-O_2.

its fingerprints in spectra) would appear or disappear. In the mixture $(N_2)_{0.92}(O_2)_{0.08}$ we discovered distinctive excitations, which are specific for the α-O_2: side band to the O_2 fundamental and the electronic transition band. So we can claim the solubility of oxygen in α^*-N_2 to be lower than 8%. In order to get a more accurate value we would have to prepare and study samples with decreasing oxygen concentration until these bands would disappear.

But there is a more time-saving way to get a solubility value. It requires an existence of the distinctive for a phase excitation, which intensity is proportional to the amount of this phase. The key of following calculations is a proportion of the phase in the mixture (relative amount of the phase), q.

A simple lever rule, demonstrated in the Fig. 18, establishes the correlation between solubility (100 − y) in % and the proportion of the phase (e.g., α^*-O_2), q. The fact that solubility of N_2 in α^*-O_2 can be considered zero makes the formula simpler. Taking in account that molar volumes of O_2-rich and N_2-rich phases are different we have:

$$q = (y - x)V_{O_2} / [xV_{N_2} + (y - x)V_{O_2}],$$

where y is a position of the solubility line at given temperature, mol% of N_2; x is a concentration of N_2 in the sample in mol%; V_{N_2} and V_{O_2} are molar volumes of α^*-N_2 and α^*-O_2 [13*,22].

The proportion of the phase q can be derived from intensities of the bands of a distinctive excitation at different concentrations but at the same temperature. This is based on a simple premise: the intensity of such band in a mixture is proportional to the effective thickness of the phase in a sample t_{eff} , which equals the sample thickness t multiplied by the proportion of that phase q. Let 100% of O_2 (pure system) be one of the concentrations then

$$I_{mix} / I_{pure} = t_{eff} / t = q,$$

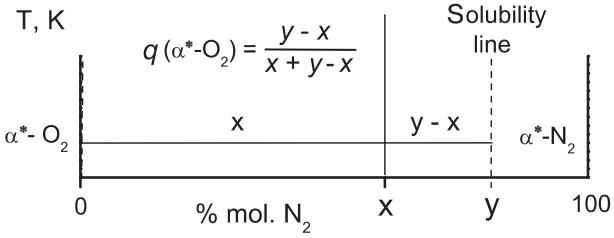

Fig. 18. Lever rule for our phase diagram.

* The authors: I.N. Krupskii, A.I. Prokhvatilov, Yu.A. Freiman, and A.I. Erenburg.

where I_{mix} and I_{pure} are intensities of the bands in mixture and in the pure.

Consequently the equation for the position of the solubility line in the phase diagram:

$$y = x\left(1 + \frac{V_{N_2}}{V_{O_2}} \frac{I_{mix}}{I_{pure} - I_{mix}}\right).$$

Thus we are able to get solubility values from the spectroscopic fingerprints of phases in our mixtures. In our case the phases are α^*- and β^*-O_2 and the distinctive excitations are O_2 side band to the fundamental and O_2 electronic absorption band. At low temperature (α^*-O_2) the side band (Fig. 19,*a*) is our choice, whereas for the β^*-O_2 phase the electronic transition band (Fig. 19,*b*) is advantageous. Such conclusion we made after we analyzed some spectroscopic features: baseline, bands' fine structure and overlapping with a spectral response from another phase.

For our lowest temperature T = 11 K we obtain y = = 96.5%. This means that about 3.5 mol% of O_2 can be solved in α^*-N_2. At T = 32 K solubility is ~ 5 mol%. An absolute error of solubility values is about ±0.5 mol%. Obtained in this way solubility line is a part of the phase diagram of Fig. 21.

This method to determine solubility can be checked comparing intensities of the excitations of N_2 molecules; these intensities must be proportional to the amount of the N_2-rich phase (α^*-N_2). In Figs. 20,*a* and 20,*b* we present spectra of two such excitations: an induced N_2 vibron band (~ 2328 cm^{-1}) and a «mixed» N_2–O_2 two-vibron band (~ 3883 cm^{-1}) in different mixtures $(N_2)_{0.55}(O_2)_{0.45}$ and $(N_2)_{0.92}(O_2)_{0.08}$ at 11 K. From the chosen sample concentration and the known solubility value (3.5% of O_2 in α^*-N_2) we calculate the relative amounts of the α^*-N_2 phase in these samples: q (α^*-N_2) = 1 − q (α^*-O_2) ≈ x/y (without consideration of molar volumes; see Fig. 18). The ratio of these values $q_{0.55}/q_{0.92}$ = 0.57/0.95 = 0.6. The ratio of the band intensities (0.65 for an induced vibron band and ~ 0.6 for a «mixed» band) must be equal in this case to the ratio of relative amounts $q_{0.55}/q_{0.92}$. Both experimental values agree pretty

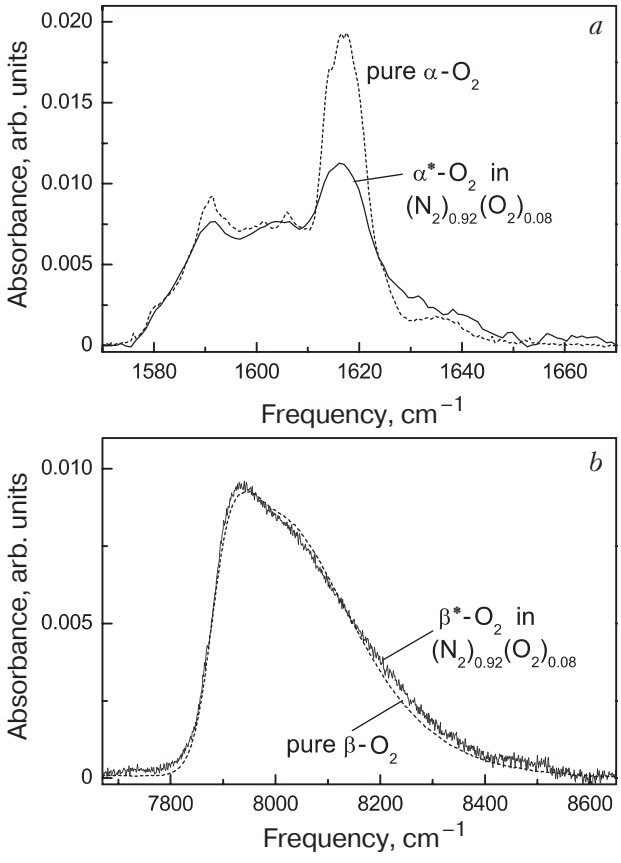

Fig. 19. Comparison of $(N_2)_{0.92}(O_2)_{0.08}$ spectra (solid line) with spectra of pure O_2 (broken line; intensities are reduced): side band to O_2 fundamental in α^*-O_2 and in α-O_2 (T = 11 K), $I_{pure}/I_{mix} \approx 30$ (*a*); O_2 electronic absorption band in β^*-O_2 and in β-O_2 (T = 26 K), $I_{pure}/I_{mix} \approx 40$ (*b*).

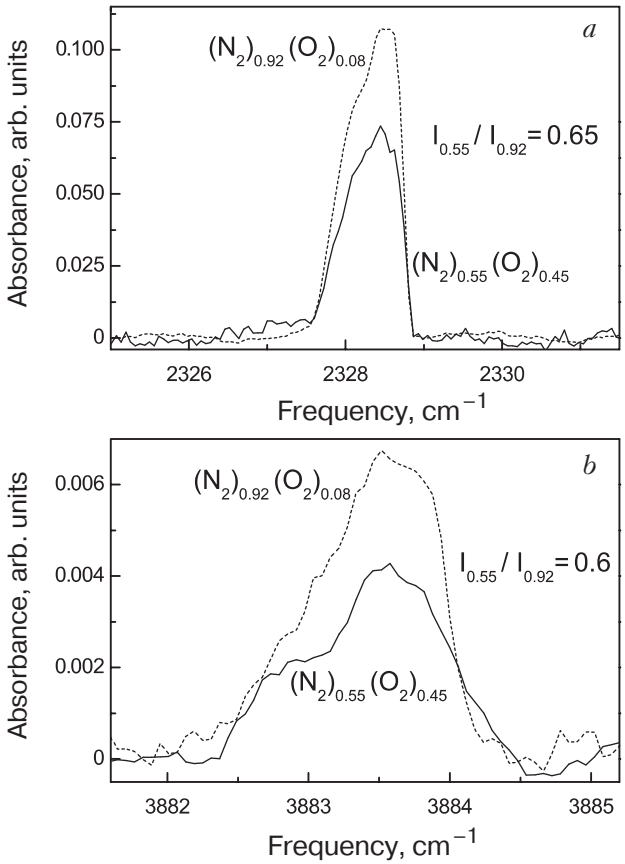

Fig. 20. Comparison of the integrated intensity of induced N_2 vibron band (*a*); and «mixed» two-vibron band between spectra of $(N_2)_{0.92}(O_2)_{0.08}$ (broken line) and $(N_2)_{0.55}(O_2)_{0.45}$ (solid line) at T = 11 K (*b*).

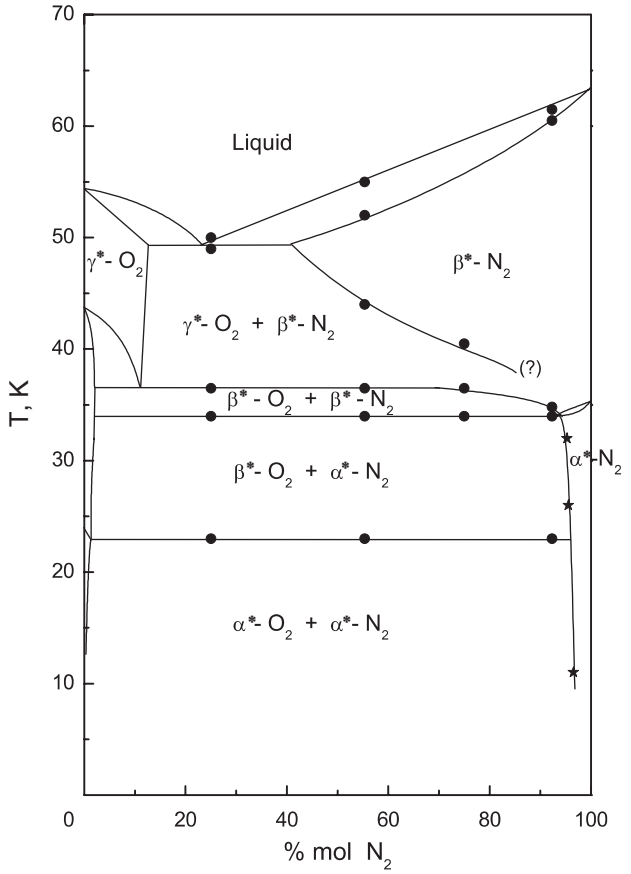

Fig. 21. Modified T–x% diagram of the N_2–O_2 binary system according to our spectroscopic studies (on the basis of Fig. 1). Closed circles — phase transitions points determined directly from changes in spectra, stars — solubility values, calculated from intensity ratios.

well with estimated ones, despite the induced character of the first band and a low intensity of the second.

Furthermore we confirmed the solubility value at T = 11 K and the solubility line in a totally different way: from spectra of matrix isolated CO (see Sec. 4.3).

Investigating thermodynamically stable samples we clarified 3 open questions: there is no X-phase; we determined a solubility line on the N_2-rich side and we measured accurate temperatures of the phase transitions. We were able to achieve one of our aims: to develop a phase diagram from fingerprints in spectra. We suggest a modified T–x% diagram of N_2–O_2 mixture (Fig. 21) that is based on results of infrared absorption studies and Raman scattering investigations.

4.2. Vibron density of states

Broad bands (~ 100 cm^{-1}), which we assigned in our spectra to phonon side bands, are similar to ones in pure systems and are well theoretically modeled [7,17]. In spectra of our mixtures these bands are just smeared out. Therefore we deal here only with narrow bands (width < 10 cm^{-1}), assigned to vibron density of states (DOS) of N_2 and O_2. In general we get information from optical spectra of Raman and infrared allowed transitions only at the center of the Brillouin zone ($\mathbf{k} \approx 0$). To scan the whole Brillouin zone one is using classically inelastic neutron scattering, which is not feasible here. Due to the symmetry of N_2 and O_2 molecules this vibration is obviously IR inactive. But in mixtures the symmetry of the molecule's environment is broken by a second component. This causes a local electric field, which induces a dipole moment, which causes an IR absorption. We profit from the fact that vibrations with all wave vectors $\mathbf{k}$, being scattered on impurities (second component), become IR active. Therefore an intensity of the resulting induced vibron band must be proportional to the vibron DOS. It is proportional as well to the concentration of second component in the phase (solubility), to a product of electric quadrupole moments of N_2 and O_2 and a distance depending term. Several spectra of induced nitrogen and oxygen vibron bands are already published [24–26], but commonly crystal quality of those samples was bad (condensation at low temperatures) and a spectral resolution was quite low.

N_2 *stretching band (~ 2330 cm^{-1}).* In Figs. 22,*a*,*b* we repeat schematically spectra in the region of the N_2 fundamental (Fig. 8) at 35 K (β^*-N_2) and at 11 K (α^*-N_2). A nearly symmetric band (width ~ 0.8 cm^{-1}) in β^*-phase, which undergoes a clear frequency jump at the phase transition, transforms into a broader asymmetric band (~ 1.3 cm^{-1}), which remains unchanged in α^*-phase. We assign these bands to the impurity induced vibron DOS of α^*- and β^*-N_2. Next we would like to discuss the band in the α^*-N_2 only.

Zumofen [27] modeled Raman spectra, especially the frequency splitting $\Delta\omega$ ($A_g - F_g$) ≈ 1.2 cm^{-1} and the intensity ratio $I(A_g)/I(T_g)$ ≈ 3:1, like in experiments [14*]. Hochstrasser [28] calculated the vibron DOS in the framework of common lattice dynamics, assuming interaction between neighboring molecules of the first and second shell (see Fig. 22,*c*, DOS). Legay [18] improved this model taking into account also the interaction of molecules of the third shell. Knorr [10] studied the mixture N_2–Ar and discussed these spectra (central peak or zero phonon line and phonon side band) in the framework of orientational glasses. Knorr modeled the central peak (ν_0) by a Gaussian line shape, whose position coincided with the Raman A_g component and whose band width decreased from 0.5 to 0.25 cm^{-1} rising temperature. At low temperature this bandwidth was interpreted as

* The authors: K.D. Bier and H.-J. Jodl.

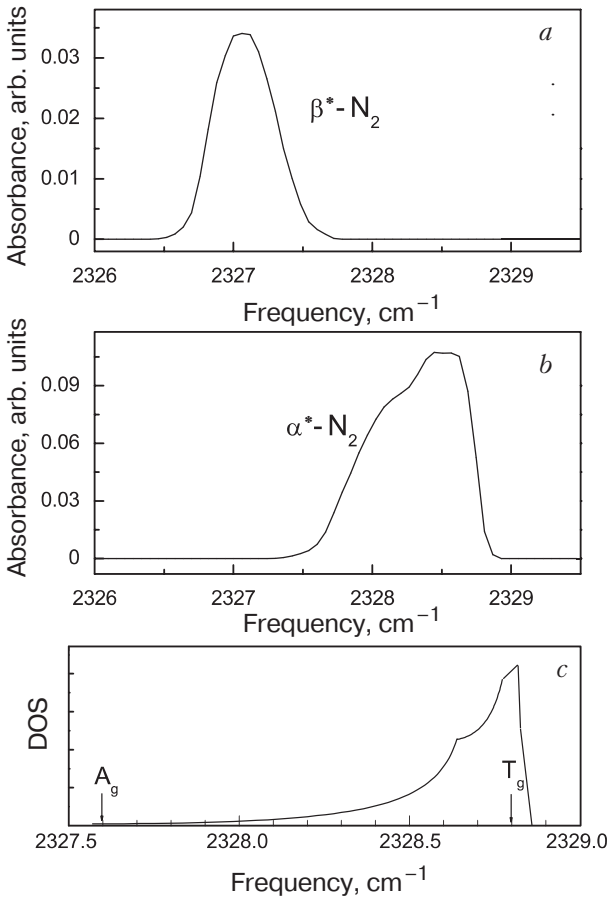

Fig. 22. Schematic N_2 vibron DOS — taken from suited spectra: β^*-N_2 at T = 35 K (*a*); α^*-N_2 at T = 11 K (*b*); modeled vibron DOS by Hochstrasser [28] and positions of Raman components (*c*).

inhomogeneously broadened due to chemical environment (mixture plus orientational disorder). The temperature dependence was explained by motional narrowing. The integrated intensity $I(T)$ was related to a glass order parameter. Raugei [29] performed MD-simulations of this N_2–Ar system and calculated a theoretical IR spectra of the ZPL plus side band; the IR intensity is impurity-induced and the bandwidth is mainly inhomogeneously broadened.

As can be seen in Fig. 22, the shape of the band in α^*-N_2 is fairly similar to the shape of the vibron DOS by Hochstrasser [28]. The obvious difference between experiment and theory is due to fact that we deal with mixtures (smearing out of singularities in DOS).

Theoretical models of the vibron DOS in β^*-N_2 are not known to us and are problematic due to orientational disorder in that phase. The increase of band intensity within β^*-N_2 during warming up (see Fig. 8) is caused by increasing solubility in this phase (more impurities lead to larger intensity of an induced band).

O_2 stretching band ($\sim$ 1550 cm^{-1}). In Figs. 23,*a*,*b*,*c* we repeat schematically spectra in the region of the O_2 fundamental (Figs. 4, 5) at 38 K (γ^*-O_2), at 24 K (β^*-O_2) and at 11 K (α^*-O_2). In spectra of $(N_2)_{0.55}(O_2)_{0.45}$ between 42–37 K (γ^*-O_2) we observe a relatively broad ($\sim$ 4 cm^{-1}) band, whose shape is not changing with temperature (Fig. 4). Its prominent narrow ($\sim$ 0.7 cm^{-1}) peak-like feature centered at around 1551 cm^{-1} is also temperature independent. This feature is similar to the induced vibron band in β^*-N_2. Whereas β-N_2 is orientationally disordered, γ-O_2 is only partly disordered and contains two types of molecules (disk-like and sphere-like).

A decrease of the band's intensity during warming is explained by a change in phases proportion in the sample: the amount of γ^*-O_2 decreases, whereas the amount of the β^*-N_2 increases. This is caused by an increase of oxygen solubility in β^*-N_2, giving simultaneously a rise to band *1* (O_2 in β^*-N_2, see Fig. 4).

In β^*-O_2 at temperatures 35–23.5 K the band shape looks completely different. It consists out of an almost triangle-like broad band ($\sim$ 7 cm^{-1}) with a $\sim$ 0.7 cm^{-1} broad feature at around 1552 cm^{-1} and a very narrow one ($<$ 0.1 cm^{-1}) at the Raman frequency 1552.5 cm^{-1}.

In α^*-O_2 below 23 K this pattern changes again (Figs. 5, 23,*c*). The broad profile ($\sim$ 7–8 cm^{-1}) becomes plateau-like now. Two new features appear: a band at 1547 cm^{-1} and an asymmetric, broad (0.2 cm^{-1}) band, with maximum at 1551.8 cm^{-1}.

A similar complex structure near the fundamental ν_0 in pure O_2 was found already by Cairns and Pimentel [24]. Later Jones [26] confirmed from studies of thin films of pure O_2 condensed at 10 K. In both cases band lost in intensity after annealing but didn't disappear. Knorr [30] observed a band in this frequency region in Ar–O_2 mixtures, but discussed it very briefly without giving an explanation. IR activity in mixtures is induced by the presence of another component. To induce the IR activity in pure O_2 one has to produce samples with a very poor optical quality, in which defects of the structure would play a role of impurities.

Unfortunately we cannot model this spectral structure by the vibron DOS of O_2 like we did before for α^*-N_2 since there are neither systematic experimental studies nor theoretical works on the vibron density of states in the α, β, γ phases of oxygen. We found in literature similar looking spectra: vibron DOS of a monolayer of CO, which is a broad asymmetric broad band with two singularities on its top [31]; vibron DOS of para-H_2 doped by ortho-H_2, which is a broad asymmetric broad band with a weak singularity at the high-frequency edge [32]; the DOS of a 2-dim honeycomb and 3-dim diamond fermionic lattice [33].

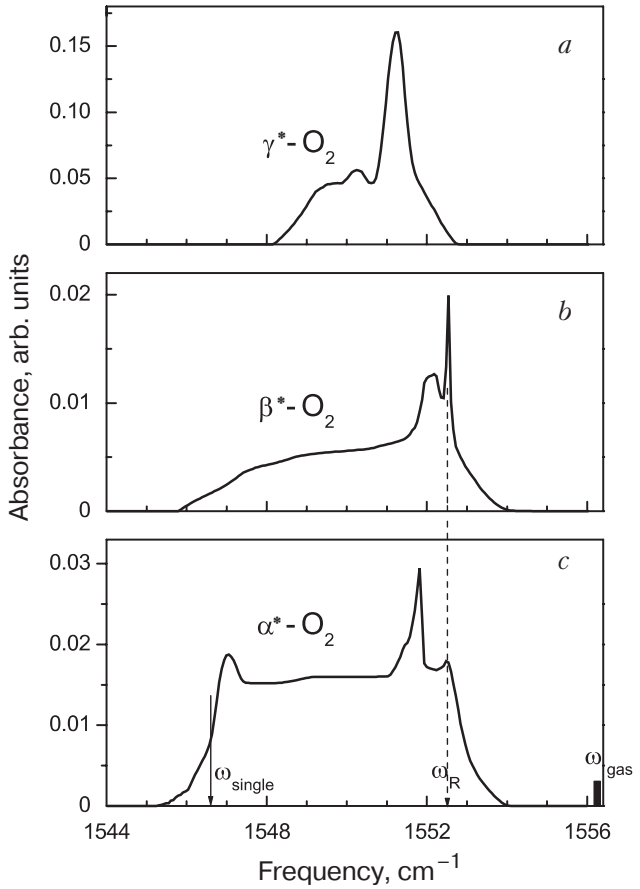

Fig. 23. Schematic O_2 vibron DOS — taken from suited spectra: γ^*-O_2 at T = 38 K (*a*); β^*-O_2 at 24 K (*b*); α^*-O_2 at 11 K (*c*). Raman frequency, gas value ([14]; the authors: H. Kiefte, M.J. Clouter, N.H. Rich, and S.F. Ahmad) and single molecule value deduced by Brodyanski [7] are shown for comparison.

The sharp asymmetric feature of the stretching band at 1551.8 cm^{-1} in our spectrum, which exists only in α^*-O_2 , looks like the 2-dim honeycomb DOS [33]. We would like to recall that α-O_2 both from crystal structure and from magnetic point of view is a quasi-2-dimensional system [34]. The structure of the basal plane is almost a honeycomb.

IR activity of the singularity at 1552.5 cm^{-1}, present in both α^*- and β^*-O_2, could be caused by a presence of lattice defects and impurities. This makes this feature dependent on crystal quality and explains its appearance in earlier IR studies of O_2 [24–26].

However the broad band ($\sim$ 4–8 cm^{-1}) seems to be characteristic for each phase (α, β, γ) and is reproducible. Therefore it cannot be simply discussed like a spectral feature, caused by defects or impurities, depending on crystal quality. According to us it mirrors the vibron DOS of oxygen phases. Unlike in α^*-, β^*-N_2 or γ^*-O_2, DOS in α^*- and β^*-O_2 are not necessarily smeared out since solubility of nitrogen in these phases is very low (< 1%). Thus, bands in Figs. 23,*b* and *c* may represent the true vibron DOS of pure β- and α-O_2.

To conclude we add some findings of Brodyanski [7] from Raman and IR studies on pure oxygen. Using the known gas phase value (1556 cm^{-1}) [14] they determined values of the environmental (D) and resonance shifts (M):

$$\omega_{\text{crystal}}\ (\mathbf{k} = 0) = \omega_{\text{gas}} + D + M = \omega_{\text{Raman}},$$

$$\omega_{\text{single}} = \omega_{\text{gas}} + D,$$

M = 6 cm^{-1} in α-O_2 (11 K), 5 cm^{-1} in β-O_2, and $\sim$ 2 cm^{-1} in γ-O_2. The resonance frequency shift is in most cases more or less the width of the vibron DOS. Widths of our vibron DOS (Fig. 23): $\sim$ 7.5 cm^{-1}, $\sim$ 7 cm^{-1}, and $\sim$ 4 cm^{-1}, respectively, that is in a fair agreement with values above.

We do hope that our experimental results, proving that oxygen vibron bands are not dispersionless, will animate theoreticians to calculate vibron DOS at least for oriented phases of oxygen.

4.3. Matrix isolated CO *fundamental (~2140 cm^{-1})*

Since the primary gases (O_2 and N_2) contain $\sim$ 2 ppm CO and since our FTIR spectrometer is sensitive enough to monitor spectra of the matrix-isolated (MI) CO fundamental at such concentrations, we can gain some information about the matrix. We have already successfully applied MI technique in solid O_2 and N_2 [35,36].

Figure 24,*a* shows spectra in the CO fundamental region as a function of temperature; one concentration $(N_2)_{0.92}(O_2)_{0.08}$ is chosen, but spectra at other examined concentrations are identical. In the interval of existence of β^*-N_2 we register only a broad (> 4 cm^{-1}) band centered at about 2139 cm^{-1}; lowering temperature we detect in α^*-N_2 4–5 narrow (< 0.3 cm^{-1}) peaks distributed between 2138.5 and 2140.5 cm^{-1}. Peak of the matrix-isolated CO in α-N_2 (T = 9 K) lies at 2139.77 cm^{-1} [37]; in oxygen (β^*- and α^*-O_2) $\sim$ 2136 cm^{-1} [35], but we detect definitely no signal (Fig. 24,*a*) there. So we deal here with the spectroscopic response from CO molecules in N_2-rich phases.

The broadening of the CO fundamental in β^*-N_2 is simply explained by the orientational disorder in this phase. But the variety of peaks in the α^*-N_2 will be discussed next.

With the knowledge of spectra at other concentrations and temperatures we were able to deconvolute the spectrum in α^*-N_2 into 5 bands (Fig. 24,*a*). The main peak (peak *3*) is centered at 2139.8 cm^{-1} (bandwidth $\sim$ 0.2 cm^{-1}) at T = 12 K, that is in agreement with the value for MI CO in N_2 in literature [37]. Therefore we assign the main peak to the IR absorp-

tion of CO molecules in α^*-N_2 surrounded by N_2 molecules only.

Taking in account that our α^*-N_2 differs from the pure α-N_2 only by the presence of 3–5% of oxygen (T = 11–32 K) and that the CO concentration is very low, what makes the discussion about CO cluster building irrelevant, we believe that this multiple structure of the CO band is caused by the presence of oxygen molecules in α^*-N_2 . A certain part of CO molecules has among 12 nearest neighbors one or more O_2 molecules. Various environments give rise to different environmental shifts that leads to a splitting of the CO band.

To achieve an assignment of all 5 peaks we analyzed their spectroscopic characteristics. In Fig. 24,*b* we plot temperature dependences of all peaks frequencies for two different concentrations $(N_2)_{0.55}$ $(O_2)_{0.45}$ and $(N_2)_{0.92}(O_2)_{0.08}$. One can recognize that frequencies of all peaks are decreasing with increasing temperature but with a different pace. The weakest temperature dependence possess peak *1* and every next one (*2*, *3*, *5*) is steeper than the previous one, whereas peak *4* behaves like peak *3*. It is worth mentioning that at the lowest temperature (11 K) the interval between peaks ($\Delta\omega_{12}$, $\Delta\omega_{23}$, $\Delta\omega_{35}$) is the same and equals 0.54 cm^{-1} (excluding peak *4*). Thus we can conclude that peaks *1*, *2*, *3* and *5* build a certain pattern.

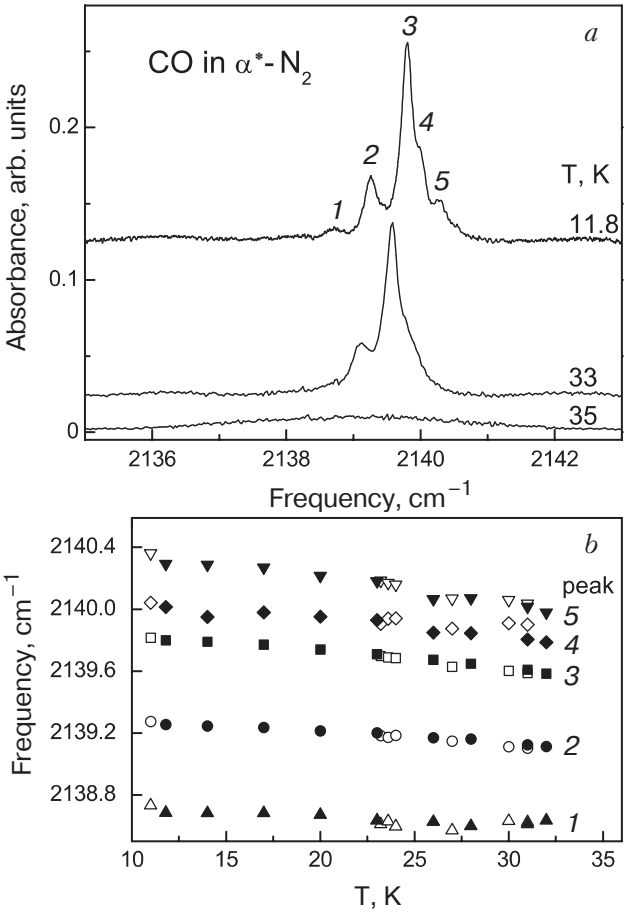

Fig. 24. Spectra in the region of the CO fundamental (~ 2140 cm^{-1}) as a function of temperature collected during warming cycle of $(N_2)_{0.92}(O_2)_{0.08}$ mixture (*a*); temperature dependence of peak maxima: peak *1* (triangles up), peak *2* (circles), peak *3* (squares), peak *4* (rhombi), peak *5* (triangles down) of two different mixtures $(N_2)_{0.92}(O_2)_{0.08}$ (full symbols) and $(N_2)_{0.55}(O_2)_{0.45}$ (open symbols) (*b*).

The following assignment is inspired by Loubeyre's article [38], in which the multiple band of H_2 embedded in Ne (also with equally spaced peaks) was convincingly modeled by taking in account different amount of the nearest neighbors of the H_2 molecule (H_2 singles, pairs, triplets, etc.). We have a slightly different situation since we have a third element (CO) probing the matrix: α^*-N_2 — a mixture of the N_2 and O_2 molecules. But the assumption of a random distribution of CO and O_2 molecules in α^*-N_2 is valid here also. So the main idea of our assignment is as follows: the CO molecules in α^*-N_2 have different number of O_2 molecules as nearest neighbors: none, one or two; the remaining neighbors are N_2 molecules.

The most intensive peak in our spectra (peak *3*, Fig. 25) we already assigned to be generated by the vibration of the CO molecules surrounded by 12 N_2 molecules as nearest neighbors in α^*-N_2; peak *2* we assign to CO surrounded by 11 N_2 and 1 oxygen molecule in the first shell, peak *1* to CO surrounded by 10 N_2 and 2 O_2. This assignment is supported by the following estimation of the frequency shifts. Frequencies of the CO absorption: in its own solid [39] at 2138.46 cm^{-1}, in α-N_2 [37] at 2139.77 cm^{-1} (shift +1.31 cm^{-1}), in α-O_2 [35] at 2135,82 cm^{-1} (shift −2.64 cm^{-1}). Number of the nearest neighbors in α^*-N_2 ($Pa3$ structure) is 12 and in α^*-O_2 ($C2/m$) is 6. So replacing one N_2 molecule by one O_2 we loose 1/12 of the N_2 frequency shift (−0.11 cm^{-1}) and gain 1/6 of the O_2 frequency shift (−0.44 cm^{-1}); the resulting shift equals −0.55 cm^{-1}. The frequency interval between peaks *1*, *2*, *3* and *5* at 11 K equals 0.54 cm^{-1}.

Returning to our assignment, peak *4*, which is shifted only by +0.2 cm^{-1} with respect to the main peak *3* and which possesses a temperature dependence identical to the one of peak *3*, is tentatively assigned by us to a splitting of the peak *3* due to broken crystal symmetry. Thus it is also a response from CO molecules surrounded by 12 N_2 molecules as the nearest neighbors.

An assignment of the remaining peak *5*, which is shifted by +0.54 cm^{-1} with respect to peak *3*, is very challenging. Following our applied model, a positive

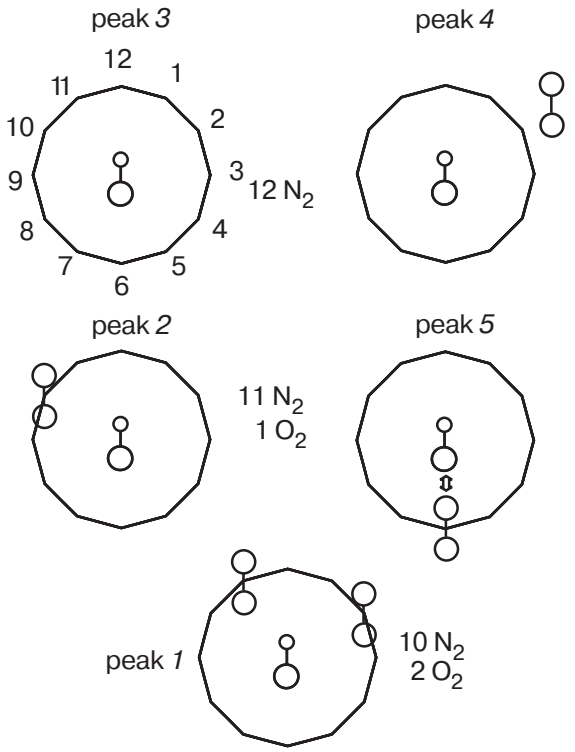

Fig. 25. Model illustrating the assignment of peaks *1–5* in the absorption spectra of CO molecules MI in α^*-N_2.

shift has the meaning of a «missing O_2 molecule» as one of the nearest neighbors. Therefore we assign peak *5* tentatively to the situation like for peak *2* (CO surrounded by 11 N_2 and 1 O_2), but in this case this O_2 molecule is very close to the O atom of the CO molecule, thus producing a positive shift due to the O-atom – O-atom repulsion.

The relative integrated intensities of the peaks do not depend on concentration and vary only weakly with temperature. Different concentrations of the samples (the lowest amount of O_2 was 8%) play no role since the ratio of the O_2 and N_2 in α^*-N_2 is given by the solubility value (3–5%), which dependence on temperature is also rather weak. At the lowest temperature (11 K) the ratio of integrated intensities is I_{p1}:I_{p2}:I_{p3}:I_{p4}:I_{p5} = 2:20:60:10:10. Increasing temperature the weaker peaks *1*, *2* and *5* gain a bit in relative intensity, while solubility of O_2 in N_2 grows too.

Although there are 5 CO peaks, they correspond only to 3 cases (Fig. 25). Between 12 nearest neighbors CO molecule can have:

1) no O_2 molecule (peaks *3* and *4*; $I_3 + I_4 = 70$);
2) one O_2 molecule (peaks *2* and *5*; $I_2 + I_5 = 30$) or
3) two O_2 molecules (peak *1*; $I_1 = 2$).

In case of a random distribution of O_2 molecules in α^*-N_2 the probability for one specific CO molecule to have no, one or two O_2 molecules as nearest neighbors depends only on the solubility of O_2 in α^*-N_2. Thus we have a good occasion to check the solubility value (3.5% at T = 11 K), obtained in Sec. 4.1. We just have to compare intensities of CO peaks corresponding to each of 3 cases (above) with mathematical probability for CO to find as neighbors of CO other molecules than N_2:

1) no O_2 ~ 64%;
2) one O_2 ~ 31%;
3) two O_2 ~ 5%.

In this respect it is a very good agreement!

Matrix isolation technique, applied in N_2–O_2 mixtures, turned out to be not only a good tool for tracing phase transitions (here (α^*–β^*)-N_2), but also a good indicator of solubility.

Conclusion

These FTIR studies on N_2–O_2 complete and confirm our Raman studies [1]. Spectra of all kinds of excitations, such as bands at O_2 (1550 cm^{-1}) and N_2 (2330 cm^{-1}) fundamentals and side bands to them, two-vibron bands (3880 cm^{-1}, 4650 cm^{-1}) and electronic transitions (8000 cm^{-1}) delivered a rich body of information. Since some of them have equivalent spectra in pure systems and are well-studied, we achieved an unambiguous assignment of spectra of our mixtures.

From fingerprints in spectra between 11 and 60 K we were able to suggest a refined T–x% diagram, which clears the inconsistencies in previous two variants: contains no mysterious X-phase, clarifies the solubility lines and possesses slightly different phase transition lines. We were able to grow thermodynamically stable samples, whose quality we have proven by optical spectra. In order to exclude the undercooling problem phase transition lines were determined during warming samples. Owing to good crystal quality and highly sensitive FTIR technique we were able (for the first time) to detect the «mixed» combined excitation (N_2 vibration + O_2 vibration); good resolved structured bands at frequencies of the fundamentals were assigned to the induced vibron DOS of N_2 or O_2; the electronic transition bands of O_2 in N_2 phases were detected as well. We have demonstrated that our method – from fingerprints in optical spectra of binary systems to T–x% phase diagram – works successfully and that we could refine the N_2–O_2 phase diagram found by structural studies. With the help of spectra of matrix isolated (~ ppm) CO molecules we probed the behavior of the matrix (e.g., phase transition) and determined independently the solubility of oxygen in α^*-N_2.

Theoretical modeling of our spectra, especially of the vibron DOS in α-, β-, γ-O_2 phases would be interesting.

Acknowledgement

We appreciate the help of A. Brodyanski during the initial stages of experiments. We thank to A. Heydt for the verification of samples concentration.

This work was supported by Deutsche Forschungsgemeinschaft (grant No. Jo 86/11).

1. M. Minenko, J. Kreutz, T. Hupprich, and H.-J. Jodl, *J. Phys. Chem.* **B108**, 6429 (2004).
2. A.S. Baryl'nik, A.I. Prokhvatilov, and L.D. Yantsevich, *Fiz. Nizk. Temp.* **15**, 501 (1989) [*Sov. J. Low Temp. Phys.* **15**, 282 (1989)]; M. Ruheman, H. Lichter, and P. Komarov, *Phys. Z. Sovjetunion* **8**, 326 (1935).
3. C.S. Barrett, L. Meyer, S.C. Greer, and J. Wasserman, *J. Chem. Phys.* **48**, 2670 (1968).
4. A.F. Prikhot'ko, V.S. Ostrovskii, V.A. Pavloshchuk, Yu.G. Pikus, P.N. Sinyavskii, and L.I. Shanskii, *Opt. Spectrosc. (USSR)* **61**, 778 (1986); V.A. Pavloshchuk, Yu.G. Pikus and L.I. Shanskii, *Opt. Spectrosc. (USSR)* **49,** 474 (1980); Yu.B. Gaididei, V.M. Loktev, A.F. Prikhot'ko, and L.I. Shanskii, *Sov. Phys. JETP* **41**, 855 (1975).
5. I.M. Pritula and L.V. Khashchina, *Fiz. Nizk. Temp.* **18**, 1035 (1992) [*Sov. J. Low Temp. Phys.* **18**, 727 (1992)].
6. Yu.A. Freiman and H.-J. Jodl, *Phys. Rep.* **401**, 1 (2004**)**; T.A. Scott, *Phys. Rep.* **27**, 89 (1976).
7. A.P. Brodyanski, S.A. Medvedev, M. Vetter, J. Kreutz, and H.-J. Jodl, *Phys. Rev.* **B66**, 104301 (2002).
8. S.A. Medvedev, A.P. Brodyanski, and H.-J. Jodl, *Phys. Rev.* **B63**, 184302 (2001).
9. D. Kivelson and P.A. Madden, *Ann. Rev. Phys. Chem.* **1980**, 1 (1980).
10. L. Jin and K. Knorr, *Phys. Rev.* **B47**, 14142 (1993); J. Xie and K. Knorr, *Phys. Rev.* **B50**, 12977 (1994).
11. W.E. Streib, T.H. Jordan, and W.N. Lipscomb, *J. Chem. Phys.* **37,** 2962 (1962); T.H. Jordan, H. W. Smith, W.E. Streib, and W.N. Lipscomb, *ibid*. **41,** 756 (1964); A.S. De Reggi, P.C. Capera, and T.A. Scott, *J. Magn. Reson*. **1,** 144 (1969).
12. A. van der Avoird, W.J. Briels, and A.P.J. Jansen, *J. Chem. Phys*. **81**, 3658 (1984).
13. I.N. Krupskii, A.I. Prokhvatilov, Yu.A. Freiman, and A.I. Erenburg, *Fiz. Nizk. Temp.* **5**, 271 (1979) [*Sov. J. Low Temp. Phys*. **5,** 130 (1979)]; A.P. Brodyanskii and Yu.A. Freiman, *Fiz. Nizk. Temp*. **11**, 994 (1985) [*Sov. J. Low Temp. Phys.* **11,** 549 (1985)].
14. H. Kiefte, M.J. Clouter, N.H. Rich, and S.F. Ahmad, *Chem. Phys. Lett*. **70**, 425 (1980); K.D. Bier and H.-J. Jodl, *J. Chem. Phys*. **81,** 1192 (1984).
15. R. Beck and J.W. Nibler, *Chem. Phys. Lett.* **159**, 79 (1989).
16. H.W. Lowen, K.D. Bier, and H.-J. Jodl, *J. Chem. Phys*. **93**, 8565 (1990).
17. G. Cardini, R. Righini, H.W. Lowen, and H.-J. Jodl, *J. Chem. Phys.* **96**, 5703 (1992).
18. F. Legay and N. Legay-Sommaire, *Chem. Phys*. **206**, 363 (1996).
19. A.P. Brodyanski, M. Vetter, S.A. Medvedev, and H.-J. Jodl (in print).
20. M. Santoro, F.A. Gorelli, L. Ulivi, R. Bini, and H.-J. Jodl, *Phys. Rev.* **B64**, 064428 (2001).
21. F.D. Medina and W.B. Daniels, *J. Chem. Phys.* **64**, 150 (1976).
22. I.N. Krupskii, A.I. Prokhvatilov, and A.I. Erenburg, *Fiz. Nizk. Temp*. **1**, 359 (1975) [*Sov. J. Low Temp. Phys*. **1**, 178 (1975)].
23. R.M. Hochstrasser and P.N. Prasad, *J. Chem. Phys.* **56**, 2814 (1972).
24. B.R. Cairns and G.C. Pimentel, *J. Chem. Phys*. **43**, 3432 (1965).
25. H.-J. Jodl, H.W. Loewen, and D. Griffith, *Solid State Commun*. **61**, 503 (1987); H.W. Lowen, K.D. Bier, and H.J. Jodl, *J. Chem. Phys*. **93**, 8565 (1990).
26. L.H. Jones, S.F. Agnew, B.I. Swanson, and S.A. Ekberg, *J. Chem. Phys*. **85**, 428 (1986).
27. G. Zumofen and K. Dressler, *J. Chem. Phys.* **64,** 5198 (1976).
28. I.I. Abram, R.M. Hochstrasser, J.E. Kohl, M.G. Semack, and D. White, *J. Chem. Phys.* **71**, 153 (1979).
29. S. Raugei, G. Cardini, V. Schettino, and H.-J. Jodl, *J. Chem. Phys.* **109,** 6382 (1998).
30. J. Xie, M. Enderle, K. Knorr, and H.-J. Jodl, *Phys. Rev.* **B55**, 8194 (1997).
31. V. Pouthier and C. Girardet, *Phys. Rev.* **B60**, 13800 (1999).
32. R.J. Hinde, *J. Chem. Phys.* **119**, 6 (2003).
33. G. Santoro, M. Airoldi, S. Sorella, and E. Tosatti, *Phys. Rev.* **B47**, 16216 (1993).
34. A.P. Brodyanski, S. Medvedev, M. Minenko, and H.-J. Jodl, in: *Frontiers of High-Pressure Research II: Application of High Pressure to Low-Dimensional Novel Electronic Materials*, *NATO Science Series*, H.D. Hochheimer, B. Kuchta, P.K. Dorhout, and J.L. Yarger, (eds.), Kluwer Academic Publishers (2001), p. 217.
35. M. Minenko, M. Vetter, A.P. Brodyanski, and H.-J. Jodl, *Fiz. Nizk. Temp*. **26,** 947 (2000) [*Low Temp. Phys*. **26,** 699 (2000)].
36. M. Vetter, M. Jordan, A.P. Brodyanski, and H.-J. Jodl, *J. Phys. Chem.* **A104,** 3698 (2000).
37. H. Dubost, R. Charneau, and M. Harig, *Chem. Phys.* **69**, 389 (1982).
38. P. Loubeyre, R. LeToullec, and J.P. Pinceaux, *Phys. Rev.* **B45**, 12844 (1992).
39. F. Legay and N. Legay-Sommaire, *Chem. Phys.* **65**, 49 (1982).